

1423
NPS67-88-001CR

NAVAL POSTGRADUATE SCHOOL

Monterey, California



CONTRACTOR REPORT

FAR FIELD COMPUTATIONAL BOUNDARY CONDITIONS

FOR INTERNAL FLOW PROBLEMS

AUGUST VERHOFF
MCDONNELL AIRCRAFT COMPANY
P.O. BOX 516
ST. LOUIS, MISSOURI 63166

SEPTEMBER 1988

APPROVED FOR PUBLIC RELEASE; DISTRIBUTION UNLIMITED.

PREPARED FOR: NAVAL POSTGRADUATE SCHOOL
MONTEREY, CALIFORNIA 93943-5000

FedDocs
D 208.14/2
NPS-67-88-001CR

DUDLEY KNOX LIBRARY
NAVAL POSTGRADUATE SCHOOL
MONTEREY, CALIFORNIA 93943

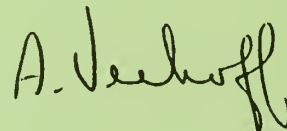
NAVAL POSTGRADUATE SCHOOL
Monterey, California

RADM R. W. West, JR.
Superintendent

H. SHULL
Provost

The present study was initiated under contract N62271-84-M-1857 during the period May 1984 to November 1984. The work was extended to the analysis of cascade flows under contract N62271-87-M-0202 during the period December 1987 to August 1988. The work was sponsored by the Air-Breathing Propulsion Research Program at Naval Air Systems Command under the cognizance of G. Derderian (AIR 931E).

This report was prepared by:



A. VERHOFF

Publication of the report does not constitute approval of the sponsor for the findings or conclusions. It is published for information and for the exchange and stimulation of ideas.

Reviewed by:

SECURITY CLASSIFICATION OF THIS PAGE

REPORT DOCUMENTATION PAGE

1 REPORT SECURITY CLASSIFICATION UNCLASSIFIED		1b RESTRICTIVE MARKINGS	
2 SECURITY CLASSIFICATION AUTHORITY		3 DISTRIBUTION / AVAILABILITY OF REPORT APPROVED FOR PUBLIC RELEASE: DISTRIBUTION IS UNLIMITED	
DECLASSIFICATION / DOWNGRADING SCHEDULE			
PERFORMING ORGANIZATION REPORT NUMBER(S) PS67-88-001CR		5 MONITORING ORGANIZATION REPORT NUMBER(S) NPS67-88-001CR	
NAME OF PERFORMING ORGANIZATION CDONNELL AIRCRAFT COMPANY	6b. OFFICE SYMBOL (If applicable)	7a NAME OF MONITORING ORGANIZATION NAVAL POSTGRADUATE SCHOOL	
ADDRESS (City, State, and ZIP Code) P.O. BOX 515 ST. LOUIS, MO 63166		7b. ADDRESS (City, State, and ZIP Code) MONTEREY, CALIFORNIA 93943-5000	
NAME OF FUNDING / SPONSORING ORGANIZATION NAVAL AIR SYSTEMS COMMAND	8b. OFFICE SYMBOL (If applicable) AIR931E	9. PROCUREMENT INSTRUMENT IDENTIFICATION NUMBER N62271-84-M-1857 N62271-87-M-0202	
ADDRESS (City, State, and ZIP Code) WASHINGTON, D.C. 20361		10. SOURCE OF FUNDING NUMBERS	
		PROGRAM ELEMENT NO. 61153N	PROJECT NO. WR024
		TASK NO. 03	WORK UNIT ACCESSION NO. 001
11. TITLE (Include Security Classification) FAR FIELD COMPUTATIONAL BOUNDARY CONDITIONS FOR INTERNAL FLOW PROBLEMS			
12. PERSONAL AUTHOR(S) BERHOFF, AUGUST			
13a. TYPE OF REPORT FINAL	13b. TIME COVERED FROM MAY 1984 TO AUG 1988	14. DATE OF REPORT (Year, Month, Day) 1988 SEPTEMBER	15. PAGE COUNT 81
16. SUPPLEMENTARY NOTATION			
COSATI CODES		18. SUBJECT TERMS (Continue on reverse if necessary and identify by block number)	
FIELD	GROUP	COMPUTATIONAL BOUNDARY CONDITIONS	
		INTERNAL FLOW COMPUTATIONS	
		CASCADE FLOW COMPUTATIONS	
17. ABSTRACT (Continue on reverse if necessary and identify by block number)			
FAR FIELD COMPUTATIONAL BOUNDARY CONDITIONS FOR 2D INTERNAL FLOW PROBLEMS ARE DEVELOPED FROM ANALYTIC SOLUTIONS OF THE LINEARIZED EULER EQUATIONS. THE EULER EQUATIONS ARE LINEARIZED ABOUT A CONSTANT PRESSURE, RECTILINEAR FLOW WHICH MAY HAVE STREAMWISE-NORMAL VARIATIONS IN TEMPERATURE AND VELOCITY AS A RESULT OF ENTROPY PRODUCTION IN THE NONLINEAR COMPUTATIONAL REGION. THE BOUNDARY PROCEDURE CAN BE USED WITH ANY NUMERICAL EULER SOLUTION METHOD AND ALLOWS COMPUTATIONAL BOUNDARIES TO BE PLACED MUCH CLOSER TO THE NONLINEAR REGION OF INTEREST.			
20. DISTRIBUTION / AVAILABILITY OF ABSTRACT <input checked="" type="checkbox"/> UNCLASSIFIED/UNLIMITED <input type="checkbox"/> SAME AS RPT <input type="checkbox"/> DTIC USERS		21. ABSTRACT SECURITY CLASSIFICATION UNCLASSIFIED	
22a. NAME OF RESPONSIBLE INDIVIDUAL R. P. SHREEVE		22b. TELEPHONE (Include Area Code) (408) 646-2593	22c. OFFICE SYMBOL 67Sf

**FAR FIELD COMPUTATIONAL BOUNDARY CONDITIONS
FOR INTERNAL FLOW PROBLEMS**

A. Verhoff

**McDonnell Aircraft Company
St. Louis, Missouri**

SEPTEMBER 1988

FAR FIELD COMPUTATIONAL BOUNDARY CONDITIONS

FOR INTERNAL FLOW PROBLEMS

A. VERHOFF

MCDONNELL AIRCRAFT COMPANY
ST. LOUIS, MISSOURI

ABSTRACT

Far field computational boundary conditions for 2D internal flow problems are developed from analytic solutions of the linearized Euler equations. The Euler equations are linearized about a constant pressure, rectilinear flow which may have streamwise-normal variations in temperature and velocity as a result of entropy production in the nonlinear computational region. The boundary procedure can be used with any numerical Euler solution method and allows computational boundaries to be placed much closer to the nonlinear region of interest.

I. INTRODUCTION

Numerical solution procedures for nonlinear fluid dynamic equations usually use one or more artificial computational boundaries located at some distance from the primary region of interest in order to limit the physical domain to finite size. If the flow crossing such a boundary (either inflow or outflow) is subsonic, then some type of computational boundary conditions must be imposed which simulate the influence of the true far field conditions at infinity. These boundary conditions must be such that waves crossing the boundary do not produce erroneous reflections back into the computational field to degrade the calculations. It is generally acknowledged that simply imposing free stream conditions (or conditions at infinity) at computational boundaries is usually inappropriate. Standard practice has consisted of locating the boundaries quite far from the region of interest in an attempt to simplify the boundary condition models and minimize any effects of inconsistent modeling. The net effect is a significant increase in the number of grid points required for an accurate flowfield calculation.

A boundary modeling procedure for two-dimensional internal flows is presented which alleviates the difficulties mentioned above and also allows the computational boundary to be located much closer to the nonlinear region of interest. The procedure is limited to steady, inviscid flow, although the flow can be rotational. It represents a logical extension of the so-called characteristic boundary conditions commonly used with inviscid numerical solution methods. Extension to axisymmetric or three-dimensional flows is straightforward.

The analysis presented here is based on the Riemann variable formulation of the Euler equations given in Reference 1. This represents a natural starting point because the characteristic (or zero-order) boundary conditions mentioned above are expressed in terms of Riemann variables. The equations are linearized about a constant pressure, rectilinear flow condition, which truly represents conditions at infinity. These linearized equations are assumed applicable in the far field region beyond a computational boundary. Within the nonlinear computational domain, strong entropy-producing (i.e.,

rotational) effects can exist which create variations in density, velocity, etc. in the far field in the streamline-normal direction which are not necessarily small perturbations. Such variations are modeled in the present analysis.

The linearized equations are solved analytically using Fourier analysis techniques as outlined in Reference 2. These solutions are coupled to the nonlinear numerical solution to provide a smooth transition across the boundary to the true far field conditions at infinity. The coupling is accomplished by the boundary conditions. The underlying principle is that the streamwise variations of both upstream and downstream running waves should decay to zero at infinity. These first-order boundary conditions provide distributions of flow quantities to be imposed along the boundary, not constant conditions. They represent a logical extension of the zero-order (or characteristic) boundary conditions. Furthermore, the boundary analysis can be coupled with any inviscid numerical solution method.

The boundary condition analysis has been applied to two-dimensional duct flow and to cascade flow, where conditions are periodic in the direction of the blade row. For duct flow, both isentropic and non-isentropic boundary conditions are derived. Only isentropic results are given for cascades. Extension to non-isentropic cascade flow can be carried out by following the procedure used for duct flow.

Numerical results are presented for both isentropic and non-isentropic duct flow. Results obtained using the first-order boundary conditions are compared with those using the zero-order boundary conditions. Numerical results for cascade flow will be presented in Reference 3. It was found that the size of the computational field and associated number of grid points needed for the nonlinear numerical solution could be reduced significantly by using the new first-order boundary condition procedure with no loss in numerical solution accuracy. The reduction in number of grid points was as much as 50 percent in some cases. The additional computational effort required by the new boundary procedure is small (less than 10 percent) so that a significant saving in overall computational effort was realized. A large portion of the gain is due to the sizeable reduction in the physical extent

the computational field and the fact that fewer solution iterations are required for information to propagate between the upstream and downstream computational boundaries leading to more rapid solution convergence.

II. PERTURBATION EQUATION DERIVATION

The system of two-dimensional, steady, linearized Euler equations which describe first-order spatial perturbations from a constant pressure state will be derived in this section. A Riemann variable formulation taken from Reference 1 will be used because of its close relationship with the characteristic (or zero-order) boundary conditions commonly used in numerical solution of the nonlinear Euler equations.

The two-dimensional form of the Euler equations is (Reference 1)

$$\frac{\partial Q}{\partial t} + (q + a) \frac{\partial Q}{\partial s} = - \frac{\gamma-1}{2} a \left(S - \frac{2}{\gamma-1} \right) \left[\frac{\partial q}{\partial s} - \frac{2}{\gamma-1} \frac{\partial a}{\partial s} \right] - \frac{\gamma-1}{2} qaS \frac{\partial \theta}{\partial n} \quad (1)$$

$$\frac{\partial R}{\partial t} + (q - a) \frac{\partial R}{\partial s} = + \frac{\gamma-1}{2} a \left(S - \frac{2}{\gamma-1} \right) \left[\frac{\partial q}{\partial s} + \frac{2}{\gamma-1} \frac{\partial a}{\partial s} \right] + \frac{\gamma-1}{2} qaS \frac{\partial \theta}{\partial n} \quad (2)$$

$$\frac{\partial \theta}{\partial t} + q \frac{\partial \theta}{\partial s} = - \frac{a^2}{\gamma q} \frac{\partial P}{\partial n} \quad (3)$$

$$\frac{\partial S}{\partial t} + q \frac{\partial S}{\partial s} = 0 \quad (4)$$

Velocity magnitude and speed of sound are denoted by q and a , respectively, and P is the logarithm of pressure. The Extended Riemann Variables Q and R are defined as

$$\begin{aligned} Q &= q + aS \\ R &= q - aS \end{aligned} \quad (5)$$

while the modified entropy is defined in terms of pressure p and density ρ as

$$S = \frac{1}{\gamma(\gamma-1)} [2\gamma - \log(p/\rho^\gamma)] \quad (6)$$

The flow angle is θ , time is denoted by t , and local distances along and normal to the streamline direction are denoted by s and n , respectively.

For steady flow the analysis can be greatly simplified by defining a new dependent variable

$$T \equiv Q - R \quad (7)$$

and replacing equations (1) and (2) by

$$(M^2 - 1) \frac{\partial T}{\partial s} + (\gamma - 1) q M S \frac{\partial \theta}{\partial n} = 0 \quad (8)$$

$$a^2 + \frac{\gamma - 1}{2} q^2 = 1 \quad (9)$$

The local Mach number is denoted by M . Equation (8) is obtained by subtracting equations (1) and (2). Equation (9) is obtained by adding equations (1) and (2) and integrating. The constant of integration, which is proportional to stagnation temperature, can be set to unity by proper choice of non-dimensionalizing quantities. The simplified form of the steady Euler equations is then

$$(M^2 - 1) \frac{\partial T}{\partial s} + (\gamma - 1) q M S \frac{\partial \theta}{\partial n} = 0 \quad (10)$$

$$M^2 \frac{\partial \theta}{\partial s} + \frac{2}{\gamma - 1} \frac{1}{T} \frac{\partial T}{\partial n} + \frac{1}{S} \left(S - \frac{2}{\gamma - 1} \right) \frac{\partial S}{\partial n} = 0 \quad (11)$$

$$\frac{\partial S}{\partial s} = 0 \quad (12)$$

$$a^2 + \frac{\gamma - 1}{2} q^2 = 1 \quad (13)$$

According to equation (12) entropy remains constant along streamlines. In regions of the flowfield where nonlinear effects are weak, the flow can be treated as a perturbation to a constant pressure, rectilinear flow. Such regions occur near and beyond far field computational boundaries. The dependent variables in equations (10)-(12) can then be expanded in asymptotic series

$$T = T_\infty + T_1 + T_2 + \dots$$

$$S = S_\infty + S_1 + S_2 + \dots \quad (14)$$

$$\theta = \theta_\infty + \theta_1 + \theta_2 + \dots$$

The flow direction at infinity is assumed constant and denoted by θ_∞ ; the perturbation quantities T_1 , S_1 and θ_1 vanish at infinity. Entropy variation is not excluded so that the flow can be rotational. Furthermore, entropy variations can be strong (i.e., not small perturbations) so that S_∞ and T_∞ are not necessarily constant, but may vary normal to the streamline direction. Note that T_∞ depends only on S_∞ (because p_∞ is constant).

Consistent with (14), spatial derivatives in equations (10)-(12) can be approximated by

$$\frac{\partial}{\partial s} = \cos \theta_\infty (1 - \tau \theta_1) \frac{\partial}{\partial x} + \cos \theta_\infty (\tau + \theta_1) \frac{\partial}{\partial y} + \dots \quad (15)$$

$$\frac{\partial}{\partial n} = -\cos \theta_\infty (\tau + \theta_1) \frac{\partial}{\partial x} + \cos \theta_\infty (1 - \tau \theta_1) \frac{\partial}{\partial y} + \dots$$

where x and y are reference Cartesian coordinates, θ is measured from the x axis, and

$$\tau \equiv \tan \theta_\infty \quad (16)$$

If expansions (14) and (15) are introduced into equations (10)-(12), the resulting first-order perturbed Euler equations are

$$(M_\infty^2 - 1) \left[\frac{\partial T_1}{\partial x} + \tau \frac{\partial T_1}{\partial y} - \theta_1 \left(\tau \frac{\partial T_\infty}{\partial x} - \frac{\partial T_\infty}{\partial y} \right) \right] + \quad (17)$$

$$(\gamma - 1) q_\infty M_\infty S_\infty \left[\frac{\partial \theta_1}{\partial y} - \tau \frac{\partial \theta_1}{\partial x} \right] = 0$$

$$\frac{\gamma - 1}{2} M_\infty^2 S_\infty \left[\frac{\partial \theta_1}{\partial x} + \tau \frac{\partial \theta_1}{\partial y} \right] + \frac{1}{2a_\infty} \left\{ \frac{\partial T_1}{\partial y} - \tau \frac{\partial T_1}{\partial x} - \frac{T_1}{T_\infty} \left[\frac{\partial T_\infty}{\partial y} - \tau \frac{\partial T_\infty}{\partial x} \right] \right\} + \quad (18)$$

$$\frac{\gamma - 1}{2} \left(S_\infty - \frac{2}{\gamma - 1} \right) \left[\frac{\partial S_1}{\partial y} - \tau \frac{\partial S_1}{\partial x} \right] + \frac{S_1}{S_\infty} \left[\frac{\partial S_\infty}{\partial y} - \tau \frac{\partial S_\infty}{\partial x} \right] = 0$$

$$\frac{\partial S_1}{\partial x} + \tau \frac{\partial S_1}{\partial y} + \theta_1 \left[\frac{\partial S_\infty}{\partial y} - \tau \frac{\partial S_\infty}{\partial x} \right] = 0 \quad (19)$$

Velocity, speed of sound, and Mach number at infinity are denoted by q_∞ , a_∞ and M_∞ , respectively, and may vary normal to the streamline direction. The fact that all dependent quantities are convected unchanged along rectilinear streamlines at infinity has been incorporated into the above equations.

Asymptotic expansions of the Riemann variables Q and R can also be defined as

$$\begin{aligned}
 Q &= Q_\infty + Q_1 + Q_2 + \dots \\
 R &= R_\infty + R_1 + R_2 + \dots
 \end{aligned}
 \tag{20}$$

Using the definition (7) and the expansion (14) for T, it follows that

$$\begin{aligned}
 T_\infty &= Q_\infty - R_\infty \\
 T_1 &= Q_1 - R_1 \\
 &\vdots \\
 &\vdots
 \end{aligned}
 \tag{21}$$

Introducing the expansions (14) and (20) into the algebraic equation (13) gives the first-order relationship

$$M_\infty (Q_1 - R_1) + \frac{\gamma - 1}{2} S_\infty M_\infty^2 (Q_1 + R_1) - 2q_\infty S_1 = 0
 \tag{22}$$

This will be used later in Section IV where the boundary conditions are derived.

III. SOLUTION OF FIRST-ORDER EQUATIONS

Solutions of the first-order equations (17)-(19) are developed in this section for two-dimensional duct flows confined by parallel walls and for infinite cascade flows. Duct flow solutions are obtained for both isentropic and non-isentropic conditions. The cascade flow solution is provided for isentropic conditions.

Duct Flow

For two-dimensional duct flow between parallel walls, the far field flow angle θ_∞ (and consequently τ) can be set to zero by aligning the coordinate x with the duct axis (see Figure 1). The width of the duct can be taken as unity without loss of generality. Equations (17)-(19) then reduce to

$$(M_\infty^2 - 1) \left[\frac{\partial T_1}{\partial x} + \theta_1 \frac{\partial T_\infty}{\partial y} \right] + (\gamma - 1) q_\infty M_\infty S_\infty \frac{\partial \theta_1}{\partial y} = 0 \quad (23)$$

$$\begin{aligned} \frac{\gamma - 1}{2} q_\infty M_\infty S_\infty \frac{\partial \theta_1}{\partial x} + \frac{1}{2} \left[\frac{\partial T_1}{\partial y} - \frac{T_1}{T_\infty} \frac{\partial T_\infty}{\partial y} \right] + a_\infty \frac{S_1}{S_\infty} \frac{\partial S_\infty}{\partial y} \\ + \frac{\gamma - 1}{2} a_\infty \left(S_\infty - \frac{2}{\gamma - 1} \right) \frac{\partial S_1}{\partial y} = 0 \end{aligned} \quad (24)$$

$$\frac{\partial S_1}{\partial x} + \theta_1 \frac{\partial S_\infty}{\partial y} = 0 \quad (25)$$

Isentropic Conditions - According to the scaled entropy definition (6), the far field entropy S_∞ is $\frac{2}{\gamma - 1}$. Equations (23)-(25) then simplify for isentropic flow to

$$\frac{\beta^2}{2q_\infty M_\infty} \frac{\partial T_1}{\partial x} - \frac{\partial \theta_1}{\partial y} = 0 \quad (26)$$

$$\frac{\partial \theta_1}{\partial x} + \frac{1}{2q_\infty M_\infty} \frac{\partial T_1}{\partial y} = 0 \quad (27)$$

where

$$\beta \equiv \sqrt{1-M_\infty^2} \quad (28)$$

Note that q_∞ and M_∞ are constant.

Equations (26) and (27) can be solved by separation of variables by assuming

$$\begin{aligned} T_1 &= 2 q_\infty M_\infty e^{\lambda x} F(y) \\ \theta_1 &= e^{\lambda x} H(y) \end{aligned} \quad (29)$$

where λ is the unknown separation constant. Equations (26) and (27) then reduce to the ordinary differential equation system

$$\begin{aligned} \beta^2 \lambda F - H' &= 0 \\ \lambda H + F' &= 0 \end{aligned} \quad (30)$$

with boundary conditions

$$H(0) = H(1) = 0 \quad (31)$$

Primes denote differentiation with respect to y . Eliminating F gives the single equation

$$H'' + \lambda^2 \beta^2 H = 0 \quad (32)$$

which has the solution

$$H = k_1 \sin \lambda \beta y + k_2 \cos \lambda \beta y \quad (33)$$

To satisfy the boundary conditions (31), the constant k_2 must be zero and

$$\lambda = \pm \frac{n\pi}{\beta} \quad (n = 1, 2, \dots) \quad (34)$$

Using these results, the general solution of the system (26) and (27) can be written as

$$\begin{bmatrix} T_1 \\ \theta_1 \end{bmatrix} = \sum_1^{\infty} K_{1n} \begin{bmatrix} \frac{2q_{\infty} M_{\infty}}{\beta} \cos n\pi y \\ \sin n\pi y \end{bmatrix} e^{n\pi x/\beta} + \sum_1^{\infty} K_{2n} \begin{bmatrix} \frac{-2q_{\infty} M_{\infty}}{\beta} \cos n\pi y \\ \sin n\pi y \end{bmatrix} e^{-n\pi x/\beta} \quad (35)$$

where K_{1n} and K_{2n} are arbitrary coefficients.

Non-Isentropic Conditions - Although the system (23)-(25) is linear, it has non-constant coefficients since S_{∞} is independent and varies with the streamline-normal direction y . The thermodynamic variables are related by

$$a_{\infty} = p_{\infty}^{\frac{\gamma-1}{2\gamma}} e^{\frac{\gamma-1}{2} \left(\frac{2}{\gamma-1} - S_{\infty} \right)} \quad (36)$$

where p_{∞} is the constant pressure at infinity.

To achieve an analytic solution, a second level of linearization can be introduced by defining a new variable $\sigma(y)$ by

$$S_{\infty} \equiv \frac{2}{\gamma-1} (1-\sigma) \quad (37)$$

Since σ is generally small, equation (36) can be approximated by

$$a_{\infty} = p_{\infty}^{\frac{\gamma-1}{2\gamma}} (1+\sigma) \quad (38)$$

An approximation for q_∞ is then provided by equation (9). Reference quantities defined by

$$\begin{aligned}\bar{a}_\infty &= p_\infty^{\frac{\gamma-1}{2\gamma}} \\ \bar{q}_\infty &= \sqrt{\frac{2}{\gamma-1} (1-\bar{a}_\infty^2)} \\ \bar{M}_\infty &= \bar{q}_\infty / \bar{a}_\infty\end{aligned}\tag{39}$$

can be introduced to simplify the notation. The approximate thermodynamic relations then become

$$\begin{aligned}a_\infty &= \bar{a}_\infty (1 + \sigma) \\ q_\infty &= \bar{q}_\infty \left(1 - \frac{2}{\gamma-1} \frac{\sigma}{\bar{M}_\infty^2}\right) \\ M_\infty &= \bar{M}_\infty \left(1 - \frac{2}{\gamma-1} \frac{\sigma}{\bar{q}_\infty^2}\right) \\ T_\infty &= \frac{4}{\gamma-1} \bar{a}_\infty\end{aligned}\tag{40}$$

All quadratic and higher terms in σ have been neglected.

Introducing the above approximations (40) into the governing equations (23)-(25) gives

$$\left(\beta^2 + \frac{4}{\gamma-1} \frac{\sigma}{\bar{a}_\infty^2}\right) \frac{\partial T_1}{\partial x} - 2\bar{q}_\infty \bar{M}_\infty \left(1 - \frac{4}{\gamma-1} \frac{\sigma}{\bar{q}_\infty^2}\right) \frac{\partial \theta_1}{\partial y} = 0\tag{41}$$

$$2\bar{q}_\infty \bar{M}_\infty \left(1 - \frac{4}{\gamma-1} \frac{\sigma}{\bar{q}_\infty^2}\right) \frac{\partial \theta_1}{\partial x} + \frac{\partial T_1}{\partial y} = 2\bar{a}_\infty \frac{\partial}{\partial y} (\sigma S_1)\tag{42}$$

$$\frac{\partial S_1}{\partial x} - \frac{2}{\gamma-1} \frac{d\sigma}{dy} \theta_1 = 0\tag{43}$$

The parameter β is defined by equation (28) with \bar{M}_∞ substituted for M_∞ . Equation (43) suggests that S_1 is of higher order than T_1 or θ_1 . If so, then the RHS of equation (42) can be set to zero and equation (43) becomes decoupled. Validity of this assumption can be verified later by evaluating numerical results obtained from this analysis. The final system of governing equations is therefore

$$\left(\beta^2 + \frac{4}{\gamma-1} \frac{\sigma}{\bar{a}_\infty^2}\right) \frac{\partial T_1}{\partial x} - 2\bar{q}_\infty \bar{M}_\infty \left(1 - \frac{4}{\gamma-1} \frac{\sigma}{\bar{q}_\infty^2}\right) \frac{\partial \theta_1}{\partial y} = 0 \quad (44)$$

$$2\bar{q}_\infty \bar{M}_\infty \left(1 - \frac{4}{\gamma-1} \frac{\sigma}{\bar{q}_\infty^2}\right) \frac{\partial \theta_1}{\partial x} + \frac{\partial T_1}{\partial y} = 0 \quad (45)$$

After these equations are solved for T_1 and θ_1 , the perturbation variable S_1 can be obtained from equation (43) by quadrature.

As for the isentropic analysis presented above, a separation of variables solution approach is again appropriate. Analogous to equations (29) assume

$$T_1 = 2\bar{q}_\infty \bar{M}_\infty e^{\lambda x} F(y) \quad (46)$$

$$\theta_1 = e^{\lambda x} H(y)$$

Equations (44) and (45) then reduce to the ordinary differential equation system

$$H' - \lambda \beta^2 F = \frac{4}{\gamma-1} \frac{\sigma}{\bar{a}_\infty^2} \left[\lambda F + \frac{1}{\bar{M}_\infty^2} H' \right] \quad (47)$$

$$F' + \lambda H = \frac{4}{\gamma-1} \frac{\sigma}{\bar{q}_\infty^2} \lambda H$$

with boundary conditions

$$H(0) = H(1) = 0 \quad (48)$$

Eliminating F from equations (47) gives the single equation

$$H'' + \lambda^2 \beta^2 H = \frac{4}{\gamma-1} \frac{1}{q_\infty^2} [\sigma(H'' + \lambda^2 \beta^2 H + \lambda \bar{M}_\infty^2 F') + \sigma'(H' + \lambda \bar{M}_\infty^2 F)] \quad (49)$$

This equation is in a form suitable for solution by iteration. The lowest order solution (i.e., first approximation) satisfies

$$H'' + \lambda^2 \beta^2 H = 0 \quad (50)$$

$$F = \frac{1}{\lambda \beta^2} H'$$

Using these results in the RHS (denoted by ϕ) of equation (49) produces

$$H'' + \lambda^2 \beta^2 H = \frac{4}{\gamma-1} \frac{1}{\beta^2 q_\infty^2} [\sigma' H' + \bar{M}_\infty^2 \sigma H''] \equiv \phi \quad (51)$$

The solution of this equation provides an improved second approximation for the solution of equation (49). Repetition of this iterative process generates ever-improving approximations. Only the solution for the second approximation will be given here. Whether or not it is sufficiently accurate can be assessed by evaluating the numerical results presented later.

The solution for the first-approximation equations (50) was obtained in the above isentropic analysis as

$$H = \sum_1^\infty A_n \sin n\pi y ; \quad \lambda = \pm \frac{n\pi}{\beta} \quad (52)$$

where the A_n are arbitrary coefficients. Note that the iterative solution procedure used here is consistent in that the isentropic solution is recovered for vanishingly small σ . Using the approximation (52) the RHS of equation (51) can be written

$$\phi = \frac{4}{\gamma-1} \frac{\pi}{\beta^2 q_\infty^2} [\sigma' \sum_1^\infty n A_n \cos n\pi y - \pi \bar{M}_\infty^2 \sigma \sum_1^\infty n^2 A_n \sin n\pi y] \quad (53)$$

Equation (51) can be separated into component equations

$$H_n'' + \lambda_n^2 \beta^2 H_n = \phi_n \quad (n = 1, 2, \dots) \quad (54)$$

where ϕ_n represents the n th component of the source term ϕ defined as

$$\phi_n = \frac{4}{\gamma-1} \frac{\pi n A_n}{\beta^2 \bar{q}_\infty^2} [\sigma' \cos n\pi y - \pi \bar{M}_\infty^2 \sigma n \sin n\pi y] \quad (55)$$

For consistency, the separation constant λ_n must also be expanded as

$$\lambda_n = \pm \left(\frac{n\pi}{\beta} + \delta\lambda_n + \dots \right) \quad (56)$$

so that equation (54) becomes

$$H_n'' + n^2 \pi^2 H_n = \phi_n - 2\pi\beta n \delta\lambda_n A_n \sin n\pi y \quad (57)$$

The solution of this equation which satisfies the boundary conditions (48) is

$$H_n = K_n \sin n\pi y + \beta \delta\lambda_n A_n y \cos n\pi y + \frac{1}{n\pi} \int_0^y \phi_n \sin n\pi(y-\eta) d\eta \quad (58)$$

where K_n is an arbitrary coefficient and

$$\delta\lambda_n = \frac{1}{n\pi\beta A_n} \int_0^1 \phi_n \sin n\pi\eta d\eta \quad (59)$$

This solution is valid regardless of the choice of sign in equation (56).

The solution for the n th component of F can be obtained from the system (47) as

$$F_n = \pm \left[\frac{K_n}{\beta} \left(1 - \frac{4}{\gamma-1} \frac{\sigma}{\beta^2 \bar{q}_\infty^2} \right) \cos n\pi y - \delta\lambda_n A_n y \sin n\pi y + \frac{1}{n\pi\beta} \int_0^y \phi_n \cos n\pi(y-\eta) d\eta \right] \quad (60)$$

The choice of sign corresponds to that of equation (56).

Using the above results, the approximate solution of the system (44) and (45) can be written as

$$\begin{aligned}
 \begin{bmatrix} T_1 \\ \theta_1 \end{bmatrix} &= \sum_1^{\infty} K_{1n} \begin{bmatrix} \frac{2\bar{q}_{\infty}\bar{M}_{\infty}}{\beta} \left(1 - \frac{4}{\gamma-1} \frac{\sigma}{\beta^2 q_{\infty}^2}\right) \cos n\pi y \\ \sin n\pi y \end{bmatrix} e^{(\frac{n\pi}{\beta} + \delta\lambda_n)x} \\
 &+ \sum_1^{\infty} K_{2n} \begin{bmatrix} \frac{-2\bar{q}_{\infty}\bar{M}_{\infty}}{\beta} \left(1 - \frac{4}{\gamma-1} \frac{\sigma}{\beta^2 q_{\infty}^2}\right) \cos n\pi y \\ \sin n\pi y \end{bmatrix} e^{-(\frac{n\pi}{\beta} + \delta\lambda_n)x} \\
 &+ \sum_1^{\infty} \begin{bmatrix} \frac{-2\bar{q}_{\infty}\bar{M}_{\infty}}{\beta} f_n \\ h_n \end{bmatrix} e^{(\frac{n\pi}{\beta} + \delta\lambda_n)x} + \sum_1^{\infty} \begin{bmatrix} \frac{2\bar{q}_{\infty}\bar{M}_{\infty}}{\beta} f_n \\ h_n \end{bmatrix} e^{-(\frac{n\pi}{\beta} + \delta\lambda_n)x}
 \end{aligned} \tag{61}$$

where

$$f_n \equiv \beta \delta\lambda_n A_n y \sin n\pi y - \frac{1}{n\pi} \int_0^y \phi_n \cos n\pi(y-\eta) d\eta \tag{62}$$

$$h_n \equiv \beta \delta\lambda_n A_n y \cos n\pi y + \frac{1}{n\pi} \int_0^y \phi_n \sin n\pi(y-\eta) d\eta \tag{63}$$

This solution reduces to the isentropic result (35) when σ is zero. Using this solution, equation (43) can be integrated to obtain the entropy perturbation S_1 .

Cascade Flow

For isentropic cascade flow, equations (17)-(19) reduce to

$$\frac{\beta^2}{2q_{\infty}\bar{M}_{\infty}} \left[\frac{\partial T_1}{\partial x} + \tau \frac{\partial T_1}{\partial y} \right] - \frac{\partial \theta_1}{\partial y} + \tau \frac{\partial \theta_1}{\partial x} = 0 \tag{64}$$

$$\frac{\partial \theta_1}{\partial x} + \tau \frac{\partial \theta_1}{\partial y} + \frac{1}{2q_\infty M_\infty} \left[\frac{\partial T_1}{\partial y} - \tau \frac{\partial T_1}{\partial x} \right] = 0 \quad (65)$$

If the (x,y) coordinates are chosen such that the flow is periodic in the y direction (see Figure 2), then a separation of variables defined as

$$\begin{aligned} T_1 &= 2q_\infty M_\infty F(\xi) e^{in\pi y} \\ \theta_1 &= H(\xi) e^{in\pi y} \\ \xi &= in\pi x \end{aligned} \quad (66)$$

can be used. The blade spacing has been taken as unity. Equations (64) and (65) are thereby transformed to the ordinary differential equation system

$$\begin{aligned} \beta^2(F' + \tau F) + \tau H' - H &= 0 \\ H' + \tau H - \tau F' + F &= 0 \end{aligned} \quad (67)$$

Primes denote differentiation with respect to ξ .

The solution of the system (67) has the form

$$F = \alpha e^{\lambda \xi} \quad H = e^{\lambda \xi} \quad (68)$$

where the eigenvalues are

$$\lambda = \frac{\tau M_\infty^2 \pm i\beta(1 + \tau^2)}{\beta^2 + \tau^2} \quad (69)$$

and

$$\alpha = \frac{\lambda + \tau}{\lambda\tau - 1} = \mp \frac{i}{\beta} \quad (70)$$

Using these results, the general solution of the system (64) and (65) can be written as

$$\begin{bmatrix} T_1 \\ \theta_1 \end{bmatrix} = \sum_{-\infty}^{\infty} K_{1n} \begin{bmatrix} \frac{-2q_{\infty} M_{\infty} i}{\beta} \\ 1 \end{bmatrix} e^{in\pi(\lambda_1 x + y)} + \sum_{-\infty}^{\infty} K_{2n} \begin{bmatrix} \frac{2q_{\infty} M_{\infty} i}{\beta} \\ 1 \end{bmatrix} e^{in\pi(\lambda_2 x + y)} \quad (71)$$

where

$$\lambda_1 \equiv \frac{\tau M_{\infty}^2 + i\beta(1 + \tau^2)}{\beta^2 + \tau^2}$$

$$\lambda_2 \equiv \frac{\tau M_{\infty}^2 - i\beta(1 + \tau^2)}{\beta^2 + \tau^2} \quad (72)$$

Note that λ_1 and λ_2 are complex conjugates.

IV. BOUNDARY CONDITION DEVELOPMENT

Examination of equations (1)-(4) shows that at a subsonic far field computational boundary there are three downstream-running waves and one upstream running wave. Therefore, the information available from the numerical solution is not complete and differs at upstream and downstream boundaries. The information lacking is provided by the boundary conditions. If the flow is supersonic, all waves are downstream-running and specification of boundary conditions is straightforward.

Far field computational boundary conditions (subsonic) are developed in this section based on the linearized Euler solutions obtained in the previous section. These solutions are assumed valid in the region beyond the computational boundaries where nonlinear effects are small. Within the computational boundaries the full nonlinear Euler equations must be solved numerically. The boundary conditions provide for a smooth coupling of the nonlinear and linear solutions so that the true conditions at infinity can be imposed.

The three specific cases analyzed in the previous section will be addressed in this section.

Duct Flow

Both upstream and downstream duct flow boundary conditions will be derived for isentropic conditions. The upstream boundary analysis is valid even if there is nonlinear entropy production downstream of the boundary within the computational domain. For non-isentropic conditions only downstream boundary conditions will be derived, since non-isentropic downstream flow is the more common situation.

For isentropic, constant pressure flow in the upstream or downstream regions, the far field Mach number M_∞ is determined implicitly from the mass flow per unit area w by the relation

$$M_\infty \left[1 + \frac{\gamma-1}{2} M_\infty^2 \right]^{\frac{1}{2}} \frac{1+\gamma}{1-\gamma} = w \quad (73)$$

The mass flow is usually known (or can be calculated) for a given duct flow problem. The associated speed of sound and velocity are

$$a_\infty = \left(\frac{M_\infty}{w} \right)^{\frac{1-\gamma}{1+\gamma}} \quad q_\infty = a_\infty M_\infty \quad (74)$$

Therefore, the far field quantities Q_∞ and R_∞ appearing in expansions (20) are

$$Q_\infty = q_\infty + \frac{2}{\gamma-1} a_\infty \quad R_\infty = q_\infty - \frac{2}{\gamma-1} a_\infty \quad (75)$$

The far field entropy has been set to $\frac{2}{\gamma-1}$. Equations (21) relate Q and R to the variable T .

For non-isentropic, constant pressure flow in the downstream region, equations (37), (39), and (40) give the approximate far field relationships

$$Q_\infty = \bar{q}_\infty + \frac{2}{\gamma-1} \bar{a}_\infty - \frac{2}{\gamma-1} \frac{\bar{a}_\infty}{M_\infty} \sigma$$

$$R_\infty = \bar{q}_\infty - \frac{2}{\gamma-1} \bar{a}_\infty - \frac{2}{\gamma-1} \frac{\bar{a}_\infty}{M_\infty} \sigma \quad (76)$$

$$T_\infty = \frac{4}{\gamma-1} \bar{a}_\infty$$

Quadratic and higher terms in σ have been neglected.

Isentropic Conditions - At a computational boundary (assumed located at $x=0$) the perturbation flow variables can be represented by the Fourier series

$$\theta_1 = \sum_1^{\infty} A_n \sin n\pi y \quad (77)$$

$$Q_1 = \sum_1^{\infty} B_n \cos n\pi y \quad (78)$$

$$R_1 = \sum_1^{\infty} C_n \cos n\pi y \quad (79)$$

$$T_1 = \sum_1^{\infty} E_n \cos n\pi y = \sum_1^{\infty} (B_n - C_n) \cos n\pi y \quad (80)$$

The boundary conditions will be developed from relationships between the Fourier coefficients A_n , B_n , and C_n . The absence of modes corresponding to $n=0$ for Q_1 , R_1 and T_1 is related to the fact that these first-order perturbations must vanish at infinity. Further discussion of this topic is presented below in conjunction with the boundary condition development for cascade flows.

The general solution for linearized isentropic flow is given by equation (35). Applying this solution at $x=0$ and using the series expansions (77)-(80) it follows that

$$A_n = K_{1n} + K_{2n} \quad (81)$$

$$E_n = \frac{2q_{\infty}M_{\infty}}{\beta} (K_{1n} - K_{2n})$$

Therefore,

$$K_{1n} = \frac{1}{2} \left[A_n + \frac{\beta}{2q_{\infty}M_{\infty}} (B_n - C_n) \right] \quad (82)$$

$$K_{2n} = \frac{1}{2} \left[A_n - \frac{\beta}{2q_{\infty}M_{\infty}} (B_n - C_n) \right] \quad (83)$$

For the region upstream of the computational boundary (i.e., $x \leq 0$), the exponentially growing component of the solution (35) can be suppressed by forcing K_{2n} to be zero. This requires the Fourier coefficients to be related by

$$A_n = \frac{\beta}{2q_\infty M_\infty} (B_n - C_n) \quad (84)$$

The linearized upstream solution is then

$$\begin{bmatrix} T_1 \\ \theta_1 \end{bmatrix} = \sum_1^\infty A_n \begin{bmatrix} \frac{2q_\infty M_\infty}{\beta} \cos n\pi y \\ \sin n\pi y \end{bmatrix} e^{n\pi x/\beta} \quad (85)$$

For isentropic flow there are two downstream-running waves propagating information to the upstream boundary from outside the computational domain and one upstream-running wave propagating information from the numerical solution. Equation (84) provides one of the lacking pieces of information from outside the computational domain; the remaining information is provided by combining equations (22), (78) and (79) to give

$$B_n = \frac{1 - M_\infty}{1 + M_\infty} C_n \quad (86)$$

Using the expansions (20) and the Fourier representation (79), the coefficients C_n are determined from

$$R_1 = \sum_1^\infty C_n \cos n\pi y = R_{num} - R_\infty \quad (87)$$

where R_{num} is the boundary distribution of R obtained from the nonlinear numerical solution and R_∞ is given by equation (75). The coefficients A_n and B_n are then obtained from equations (84) and (86). Using the Fourier representations (77) and (78), the distributions of θ and Q on the boundary (i.e., the boundary conditions) are calculated according to

$$\theta_b = \sum_1^\infty A_n \sin n\pi y \quad (88)$$

$$Q_b = Q_\infty + \sum_1^\infty B_n \cos n\pi y$$

For the region downstream of the computational boundary (i.e., $x \geq 0$), the exponentially growing component of the solution (35) can be suppressed by forcing K_{1n} defined by equation (82) to be zero. This requires the Fourier coefficients to be related by

$$C_n = B_n + \frac{2q_\infty M_\infty}{\beta} A_n \quad (89)$$

The linearized downstream solution is then

$$\begin{bmatrix} T_1 \\ \theta_1 \end{bmatrix} = \sum_1^\infty A_n \begin{bmatrix} \frac{-2q_\infty M_\infty}{\beta} \cos n\pi y \\ \sin n\pi y \end{bmatrix} e^{-n\pi x/\beta} \quad (90)$$

For isentropic flow there are two downstream-running waves propagating information to the downstream boundary from the numerical solution and one upstream-running wave propagating information from outside the computational domain. Equation (89) provides the lacking information. Using the expansion (20) and the Fourier representations (77) and (78), the coefficients A_n and B_n are determined from

$$\theta_1 = \sum_1^\infty A_n \sin n\pi y = \theta_{num} \quad (91)$$

$$Q_1 = \sum_1^\infty B_n \cos n\pi y = Q_{num} - Q_\infty$$

where θ_{num} and Q_{num} are the boundary distributions of θ and Q obtained from the nonlinear numerical solution and Q_∞ is given by equations (75). The coefficients C_n are then obtained from equation (89). Using the Fourier representation (79), the distribution of R on the boundary (i.e., the boundary condition) is calculated according to

$$\begin{aligned} R_b &= R_\infty + \sum_1^\infty C_n \cos n\pi y \\ &= Q_{num} - \frac{4}{\gamma-1} a_\infty + \frac{2q_\infty M_\infty}{\beta} \sum_1^\infty A_n \cos n\pi y \end{aligned} \quad (92)$$

The second form of this relation requires only the calculation of the coefficients A_n .

Many numerical solution algorithms for the Euler equations use so-called characteristic far field boundary conditions in which θ_∞ and Q_∞ are specified at inflow boundaries and R_∞ is imposed at outflow boundaries. The boundary conditions (88) and (92) therefore represent a logical first-order extension of the widely-used characteristic (or zero-order) boundary conditions.

Non-Isentropic Conditions - For the case of non-isentropic flow crossing a downstream computational boundary, the Fourier series representation (77) for θ_1 at the boundary is still valid because θ is zero at the duct walls. The variable σ which characterizes the entropy distribution at infinity can be represented by

$$\sigma = \sigma_w + \sum_1^{\infty} D_k \sin(k-1/2)\pi y \quad (93)$$

where σ_w is the wall value at $y = 0$. This Fourier series representation assumes an even extension of σ for $1 \leq y \leq 2$. The source term component ϕ_n defined by equation (55) can then be written as

$$\begin{aligned} \phi_n = \frac{2}{\gamma-1} \frac{n\pi^2 A_n}{\beta^2 q_\infty^2} \left\{ \sum_{k=1}^{\infty} (k-1/2) D_k [\cos(n+k-1/2)\pi y + \cos(n-k+1/2)\pi y] \right. \\ \left. + n \bar{M}_\infty^2 \sum_{k=1}^{\infty} D_k [\cos(n+k-1/2)\pi y - \cos(n-k+1/2)\pi y] - 2\sigma_w \bar{M}_\infty^2 n \sin n\pi y \right\} \end{aligned} \quad (94)$$

The procedure for relating σ to the entropy distribution at the computational boundary and determining the coefficients D_k will be presented later.

The approximate solution for linearized non-isentropic flow is given by equation (61). Since it is only an approximate solution of the approximate system (44) and (45), the arguments used in the isentropic analysis for choosing K_{1n} and K_{2n} to eliminate exponentially growing solution components cannot be used. That is, the RHS of equation (51) has been treated as a known source term by using a lower-order solution approximation. As a result, the

behavior of the source term for large x directly influences the character of the solution obtained. However, closer examination of the isentropic analysis shows that the same results would have been obtained had the exponentially growing components simply been ignored. The remaining constant (i.e., K_{1n} or K_{2n}) associated with the decaying solution component could have been determined by matching the solution at $x=0$ with the Fourier series representations on the boundary.

Using this approach and selecting only the decaying component of the solution (61), the solution for the downstream region (i.e., $x \geq 0$) is

$$\begin{aligned} \begin{bmatrix} T_1 \\ \theta_1 \end{bmatrix} &= \sum_1^{\infty} K_n \begin{bmatrix} \frac{-2\bar{q}_{\infty}\bar{M}_{\infty}}{\beta} \left(1 - \frac{4}{\gamma-1} \frac{\sigma}{\beta 2\bar{q}_{\infty}^2}\right) \cos n\pi y \\ \sin n\pi y \end{bmatrix} e^{-\left(\frac{n\pi}{\beta} + \delta\lambda_n\right)x} \\ &+ \sum_1^{\infty} \begin{bmatrix} \frac{2\bar{q}_{\infty}\bar{M}_{\infty}}{\beta} f_n \\ h_n \end{bmatrix} e^{-\left(\frac{n\pi}{\beta} + \delta\lambda_n\right)x} \end{aligned} \quad (95)$$

where

$$f_n = \beta \delta\lambda_n A_n y \sin n\pi y - \frac{1}{n\pi} \int_0^y \phi_n \cos n\pi(y-\eta) d\eta \quad (96)$$

$$h_n = \beta \delta\lambda_n A_n y \cos n\pi y + \frac{1}{n\pi} \int_0^y \phi_n \sin n\pi(y-\eta) d\eta \quad (97)$$

$$\delta\lambda_n = \frac{1}{n\pi\beta A_n} \int_0^1 \phi_n \sin n\pi\eta d\eta \quad (98)$$

These last three expressions are obtained from equations (59), (62), and (63). If the upstream region (i.e., $x < 0$) were to be analyzed for non-isentropic conditions, then the other solution component would need to be selected.

The solution (95) can be matched to conditions at the computational boundary $x=0$ by letting

$$K_n = A_n + \delta A_n \quad (99)$$

and using the Fourier series representation (77) to give

$$\begin{aligned} \delta A_m = & \sum_{n=1}^{\infty} \frac{2}{n\pi} \int_0^1 \sin m\pi y \int_0^y \phi_n \sin n\pi(\eta-y) d\eta dy - \\ & 2\beta \sum_{n=1}^{\infty} A_n \delta\lambda_n \int_0^1 \sin m\pi y \cos n\pi y y dy \end{aligned} \quad (100)$$

Evaluation of the integrals in this expression along with those appearing in equations (96)-(98) is given in Appendix A.

All parameters appearing in the solution (95) can be evaluated in terms of the Fourier coefficients A_n and D_k . The A_n coefficients can be determined in the same manner as for isentropic flow using equation (91), namely,

$$\sum_1^{\infty} A_n \sin n\pi y = \theta_{num} \quad (101)$$

where θ_{num} is the distribution of θ along the boundary obtained from the nonlinear numerical solution. The D_k coefficients can be determined by solving the entropy equation (43). Neglecting higher-order terms, its solution is

$$S_1 = - \frac{2}{\gamma-1} \frac{\beta}{\pi} \frac{d\sigma}{dy} \sum_1^{\infty} \frac{A_n}{n} \sin n\pi y e^{-\left(\frac{n\pi}{\beta} + \delta\lambda_n\right)x} \quad (102)$$

where, from equation (93),

$$\frac{d\sigma}{dy} = \pi \sum_1^{\infty} (k-1/2) D_k \cos(k-1/2)\pi y \quad (103)$$

Combining these two expressions gives

$$S_1 = - \frac{\beta}{\gamma-1} \sum_{k=1}^{\infty} \sum_{n=1}^{\infty} \frac{k-1/2}{n} A_n D_k [\sin(n+k-1/2)\pi y + \sin(n-k+1/2)\pi y] e^{-(\frac{n\pi}{\beta} + \delta\lambda_n)x} \quad (104)$$

Since entropy is convected downstream along streamlines, the distribution at the computational boundary, denoted by S_{num} , is known from the numerical solution. From the expansions (14) and the definition (37) it follows that

$$\begin{aligned} S_{num} &= S_{\infty} + S_1(0,y) \\ &= \frac{2}{\gamma-1} (1 - \sigma) + S_1(0,y) \end{aligned} \quad (105)$$

Introducing the relationship (93) for σ and $S_1(0,y)$ from the solution (104) gives

$$\sum_{k=1}^{\infty} D_k \sin(k-1/2)\pi y = 1 - \sigma_w - \frac{\gamma-1}{2} S_{num} - \quad (106)$$

$$\frac{\beta}{2} \sum_{k=1}^{\infty} \sum_{n=1}^{\infty} \frac{k-1/2}{n} A_n D_k [\sin(n+k-1/2)\pi y + \sin(n-k+1/2)\pi y]$$

The coefficients D_k must therefore satisfy

$$D_m = 2 \int_0^1 [1 - \sigma_w - \frac{\gamma-1}{2} S_{num}] \sin(m-1/2)\pi y dy - \quad (107)$$

$$\frac{\beta}{2} \sum_{k=1}^{m-1} \frac{k-1/2}{m-k} D_k A_{m-k} - \frac{\beta}{2} \sum_{k=1}^{\infty} \frac{k-1/2}{m+k-1} D_k A_{m+k-1} + \frac{\beta}{2} \sum_{k=m+1}^{\infty} \frac{k-1/2}{k-m} D_k A_{k-m}$$

This equation can be solved for each D_m by iteration, started by using the first integral term as an initial guess. Note that the wall value σ_w is known from the numerical solution since the wall is a streamline.

Combining the definition (7) and the expansions (14) gives the first-order relation

$$R = Q - T_\infty - T_1 \quad (108)$$

Applying this approximation along with the solution (95) at the computational boundary $x=0$, the distribution of R on the boundary (i.e., the boundary condition) can be calculated according to

$$R_b = Q_{num} - \frac{4}{\gamma-1} \bar{a}_\infty + \frac{2\bar{q}_\infty \bar{M}_\infty}{\beta} \left(1 - \frac{4}{\gamma-1} \frac{\sigma}{\beta 2\bar{q}_\infty^2}\right) \sum_1^\infty (A_n + \delta A_n) \cos n\pi y$$

$$- \frac{2\bar{q}_\infty \bar{M}_\infty}{\beta} \sum_1^\infty f_n \quad (109)$$

The approximation (76) for T_∞ has been used and Q_{num} denotes the boundary distribution of Q obtained from the nonlinear numerical solution. This expression reduces to the boundary condition (92) if the flow becomes isentropic.

Cascade Flow

Both upstream and downstream cascade boundary conditions will be derived for isentropic conditions. The analysis parallels that for isentropic duct flow except that the parameters appearing in the general linearized solution (71) are complex quantities. For isentropic conditions, the cascade turns the flow without losses. Therefore, all upstream and downstream far field quantities (e.g., Q_∞ , R_∞ , etc.) can be determined from the downstream pressure at infinity, p_∞ .

At a computation boundary (assumed located at $x=0$) the perturbation flow variables can be represented by the general Fourier series

$$\begin{aligned} \theta_1 &= \sum_{-\infty}^{\infty} A_n e^{in\pi y} \\ &= \frac{\bar{A}_0}{2} + \sum_1^{\infty} \bar{A}_n \cos n\pi y + \sum_1^{\infty} \tilde{A}_n \sin n\pi y \end{aligned} \tag{110}$$

$$\begin{aligned} Q_1 &= \sum_{-\infty}^{\infty} B_n e^{in\pi y} \\ &= \frac{\bar{B}_0}{2} + \sum_1^{\infty} \bar{B}_n \cos n\pi y + \sum_1^{\infty} \tilde{B}_n \sin n\pi y \end{aligned} \tag{111}$$

$$\begin{aligned} R_1 &= \sum_{-\infty}^{\infty} C_n e^{in\pi y} \\ &= \frac{\bar{C}_0}{2} + \sum_1^{\infty} \bar{C}_n \cos n\pi y + \sum_1^{\infty} \tilde{C}_n \sin n\pi y \end{aligned} \tag{112}$$

$$\begin{aligned} T_1 &= \sum_{-\infty}^{\infty} E_n e^{in\pi y} \\ &= \frac{\bar{E}_0}{2} + \sum_1^{\infty} \bar{E}_n \cos n\pi y + \sum_1^{\infty} \tilde{E}_n \sin n\pi y \end{aligned} \tag{113}$$

The boundary conditions will be developed from relationships between the Fourier coefficients A_n , B_n and C_n . Fourier analysis provides the additional relationships (for $n = 0, 1, 2, \dots$)

$$\begin{aligned} \bar{Z}_n &= Z_n + Z_{-n} & Z_n &= \frac{1}{2} (\bar{Z}_n - i \tilde{Z}_n) \\ \tilde{Z}_n &= i (Z_n - Z_{-n}) & Z_{-n} &= \frac{1}{2} (\bar{Z}_n + i \tilde{Z}_n) \end{aligned} \tag{114}$$

where Z represents any of the coefficients A , B , C or E . Since perturbations must vanish at infinity, \bar{A}_0 , \bar{B}_0 , \bar{C}_0 and \bar{E}_0 must each be zero.

Applying the solution (71) at $x=0$ and using the series expansions (110) and (113) it follows that

$$A_n = K_{1n} + K_{2n} \quad (115)$$

$$E_n = \frac{2q_\infty M_\infty}{\beta} i (K_{2n} - K_{1n})$$

Therefore,

$$K_{1n} = \frac{1}{2} \left[A_n + \frac{i\beta}{2q_\infty M_\infty} E_n \right] \quad (116)$$

$$K_{2n} = \frac{1}{2} \left[A_n - \frac{i\beta}{2q_\infty M_\infty} E_n \right] \quad (117)$$

In the region upstream of the computational boundary (i.e., $x \leq 0$) the inflow angle θ_∞ is known so that τ defined by equation (16) is known. To suppress the exponentially growing component of the solution (71), the coefficients K_{1n} and K_{2n} must satisfy

$$K_{1n} = 0 \quad (n > 0) \quad \quad \quad K_{2n} = 0 \quad (n < 0) \quad (118)$$

This requires the Fourier coefficients to be related by

$$A_n = -\frac{i\beta}{2q_\infty M_\infty} E_n = -\frac{i\beta}{2q_\infty M_\infty} (B_n - C_n) \quad (n > 0) \quad (119)$$

$$A_n = \frac{i\beta}{2q_\infty M_\infty} E_n = \frac{i\beta}{2q_\infty M_\infty} (B_n - C_n) \quad (n < 0)$$

The linearized upstream solution is then

$$\begin{bmatrix} T_1 \\ \theta_1 \end{bmatrix} = \sum_{-\infty}^{-1} A_n \begin{bmatrix} -2q_\infty M_\infty i \\ \beta \\ 1 \end{bmatrix} e^{in\pi(\lambda_1 x + y)} + \sum_1^{\infty} A_n \begin{bmatrix} 2q_\infty M_\infty i \\ \beta \\ 1 \end{bmatrix} e^{in\pi(\lambda_2 x + y)} \quad (120)$$

The parameters λ_1 and λ_2 are defined by equations (72). The component corresponding to $n=0$ has been neglected. This will be discussed in more detail below.

Equation (86) used for the duct flow analysis is again applicable. Equation (87) can be generalized to determine the coefficients C_n . That is, \bar{C}_n and \tilde{C}_n are determined from

$$\sum_1^{\infty} \bar{C}_n \cos n\pi y + \sum_1^{\infty} \tilde{C}_n \sin n\pi y = R_{num} - R_{\infty} \quad (121)$$

where R_{num} is the boundary distribution of R obtained from the nonlinear numerical solution. The coefficient \bar{C}_0 has been neglected. The coefficients A_n and B_n are then obtained from equations (86) and (119) and the general Fourier relationships (114). Using the Fourier representations (110) and (111), the distributions of θ and Q on the boundary (i.e., the boundary conditions) are calculated according to

$$\begin{aligned} \theta_b &= \theta_{\infty} + \sum_1^{\infty} \bar{A}_n \cos n\pi y + \sum_1^{\infty} \tilde{A}_n \sin n\pi y \\ Q_b &= Q_{\infty} + \sum_1^{\infty} \bar{B}_n \cos n\pi y + \sum_1^{\infty} \tilde{B}_n \sin n\pi y \end{aligned} \quad (122)$$

Both \bar{A}_0 and \bar{B}_0 have been set to zero in the boundary conditions (122). A zero value of \bar{B}_0 imposed on the numerical solution through the boundary condition should tend to force a zero value for \bar{C}_0 (and hence \bar{E}_0) in the numerical solution according to equation (86). It should be noted from these first-order relations that, within the context of a Fourier representation, Q_{∞} and θ_{∞} can be viewed as the mean values of Q and θ on the computational boundary. Deviations from this condition can be shown to be a second-order effect. These arguments apply also to duct flows.

For the region downstream of the computational boundary (i.e., $x \geq 0$), the outflow angle θ_∞ is unknown so that τ is also unknown. To suppress the exponentially growing component of the solution (71), the coefficients K_{1n} and K_{2n} must satisfy

$$K_{1n} = 0 \quad (n < 0) \qquad K_{2n} = 0 \quad (n > 0) \qquad (123)$$

This requires the Fourier coefficients to be related by

$$A_n = -\frac{i\beta}{2q_\infty M_\infty} E_n = -\frac{i\beta}{2q_\infty M_\infty} (B_n - C_n) \quad (n < 0) \qquad (124)$$

$$A_n = \frac{i\beta}{2q_\infty M_\infty} E_n = \frac{i\beta}{2q_\infty M_\infty} (B_n - C_n) \quad (n > 0)$$

The linearized downstream solution is then

$$\begin{bmatrix} T \\ \theta_1 \end{bmatrix} = \sum_1^{\infty} A_n \begin{bmatrix} -2q_\infty M_\infty i \\ \beta \\ 1 \end{bmatrix} e^{in\pi(\lambda_1 x + y)} + \sum_{-\infty}^{-1} A_n \begin{bmatrix} 2q_\infty M_\infty i \\ \beta \\ 1 \end{bmatrix} e^{in\pi(\lambda_2 x + y)} \qquad (125)$$

As for the duct flow analysis, the coefficients A_n and B_n are determined from the general Fourier representations (110) and (111) according to

$$\sum_1^{\infty} \bar{A}_n \cos n\pi y + \sum_1^{\infty} \bar{A}_n \sin n\pi y = \theta_{num} - \theta_\infty \qquad (126)$$

$$\sum_1^{\infty} \bar{B}_n \cos n\pi y + \sum_1^{\infty} \bar{B}_n \sin n\pi y = Q_{num} - Q_\infty$$

where θ_{num} and Q_{num} are the boundary distributions of θ and Q obtained from the nonlinear numerical solution. The coefficients \bar{A}_0 and \bar{B}_0 have been neglected. The outflow angle θ_∞ can be calculated from

$$\theta_{\infty} = \int_0^1 \theta_{\text{num}} dy \quad (127)$$

which is the mean value of θ on the boundary. This justifies setting the coefficient \bar{A}_0 to zero. The coefficients C_n are obtained from equations (124). Using the Fourier representation (112), the distribution of R on the boundary (i.e., the boundary condition) is calculated from

$$\begin{aligned} R_b &= R_{\infty} + \sum_1^{\infty} \bar{C}_n \cos n\pi y + \sum_1^{\infty} \tilde{C}_n \sin n\pi y \\ &= Q_{\text{num}} - \frac{4}{\gamma-1} a_{\infty} + \frac{2q_{\infty}M_{\infty}}{\beta} \left[\sum_1^{\infty} \tilde{A}_n \cos n\pi y - \sum_1^{\infty} \bar{A}_n \sin n\pi y \right] \end{aligned} \quad (128)$$

The second form of this relation requires only the evaluation of the coefficients \bar{A}_n and \tilde{A}_n . It is analogous to equation (92) for duct flow.

The coefficient \bar{C}_0 has been set to zero which, when imposed on the numerical solution through the boundary condition, should tend to force a zero value for \bar{B}_0 (and hence \bar{E}_0). That is, the boundary condition tends to enforce R_{∞} as the mean value of R on the boundary. This argument applies also to duct flows.

V. APPLICATIONS

Numerical solutions of the Euler equations have been calculated for two-dimensional, steady duct flows using the first-order boundary condition procedures developed in the previous section. Both isentropic and non-isentropic cases were analyzed. Non-isentropic flow was produced by a shock wave located in a nozzle portion of the duct. First-order boundary condition results are compared with those produced using the conventional zero-order characteristic boundary conditions.

A solution algorithm was used for the nonlinear Euler equations (1)-(4) which is based on the method presented in Reference 1. It uses explicit time integration to relax to steady state conditions and includes the shock-fitting procedure of Reference 4 to accurately calculate flows containing shock waves. Shock waves appear in the solution as distinct discontinuities which satisfy the Rankine-Hugoniot relations. It should be noted that the boundary condition analysis is independent of the choice of inviscid, nonlinear solution method.

The duct/nozzle geometry is shown schematically in Figure 1. The flow is characterized by p_∞ , the downstream pressure at infinity, which produces a mass flow per unit area w through the duct. The linearized solutions given by equations (85), (90) and (95) are assumed valid in the semi-infinite regions I and III and the computational boundary conditions are applied at the upstream and downstream boundaries AA and BB of the nonlinear computational region II.

The actual shape of the duct/nozzle and the computational grid are shown in Figure 3. The nozzle contour is sinusoidal and symmetric about the centerline. The computational grid for this portion of the nozzle had dimensions 41 x 21. The area ratio is .75 and the upstream and downstream areas are equal. For these constant area sections of the duct, additional rectangular grid cells could be added without altering the basic 41 x 21 grid. This served to minimize the effect of grid changes on the calculations when the computational boundaries were moved in order to assess the accuracy of the boundary conditions.

Because the configuration is symmetric, calculations were limited to the lower half of the duct and a centerline symmetry condition was used. Although the configuration used for these calculations is simple, the boundary condition analysis of the previous section is general and applicable to unsymmetric configurations having unequal upstream and downstream areas. Use of the simple configuration is sufficient to demonstrate the validity of the analysis.

Isentropic Conditions

For isentropic flow the first-order upstream and downstream boundary conditions are given by equations (88) and (92), respectively. The associated analytic far field solutions are given by equations (85) and (90). The zero-order (or characteristic) boundary conditions consist of imposing the constant value of Q_∞ and a zero value of θ along the upstream boundary and the constant value of R_∞ along the downstream boundary. The values of Q_∞ and R_∞ are determined from equations (74) and (75).

Results are presented for a single value of p_∞ but with the computational boundaries located at several different longitudinal stations. The relative accuracy of the zero and first-order boundary conditions can then be evaluated.

Case 1 - Results obtained using the complete grid shown in Figure 3 are presented in Figures 4 and 5. This grid has 20 columns of grid cells in both the upstream and downstream constant area portions of the duct. For this case the computational boundaries were far enough upstream and downstream that the zero-order and first-order boundary condition results were nearly identical. Figure 4 shows pressure and Mach number distributions along the centerline and lower wall of the duct/nozzle. Pressure, Mach number, and flow angle contours are presented in Figure 5. These results serve as a reference for evaluating the accuracy of solutions where the computational boundaries are moved closer to the nozzle portion of the duct.

Case 2 - Results for a shortened duct obtained using the zero-order boundary conditions are presented in Figure 6 and 7. There were 5 columns of grid

cells in both the upstream and downstream constant area portions of the duct for this case. Pressure and Mach number distributions are shown in Figure 6 and contours are shown in Figure 7. The most noticeable effect of the boundary proximity is a change in peak values of pressure and Mach number and a significant amount of longitudinal asymmetry.

Case 3 - The previous shortened duct case was recalculated using the first-order boundary conditions. These results are presented in Figures 8 and 9. Pressure and Mach number distributions are shown in Figure 8 and contours are shown in Figure 9. The results within the numerical solution portion of the domain are almost identical to those shown in Figures 4 and 5. Linearized solution results obtained from equations (85) and (90) have been added upstream and downstream of the computational boundaries. It is evident that the linearized far field analytic solutions provide for a smooth transition across the computational boundary to the true far field conditions at infinity.

Case 4 - Results for a more drastic case using the first-order boundary conditions are presented in Figures 10 and 11. Only one column of grid cells was used in the upstream and downstream constant-area portions of the duct. Pressure and Mach number distributions are shown in Figure 10 and contours in Figure 11. Even with the computational boundaries extremely close, the numerical solution in the nozzle portion of the duct is affected very little.

Boundary Comparison - A more quantitative comparison between the zero- and first-order boundary conditions can be obtained by examining the distribution of flow variables along the computational boundaries. Figure 12 shows a comparison of the distribution of pressure and flow angle along the upstream and downstream boundaries for Cases 2 and 3. Results taken from the numerical solution of Case 1 at the same longitudinal locations are also shown. There is little difference between the Case 1 and Case 3 results. The larger differences between the Case 2 and Case 3 pressures occurring along the upstream boundary are primarily due to the fact that a zero flow angle is imposed along the boundary.

Implementation of the first-order boundary conditions obviously introduces additional computational effort. However, the boundary conditions do not have to be updated with every iteration of the numerical solution. The small additional effort is more than offset by the large reduction in number of grid points required and the fewer solution iterations necessary for convergence because information propagates between the computational boundaries more quickly. For the isentropic results presented above, only 5 Fourier modes were required to give a reasonably accurate representation of the boundary distributions of R (upstream) and θ (downstream) for the Case 3 calculations. For the Case 1 and Case 4 calculations, the number of Fourier modes required were 3 and 7, respectively.

Non-Isentropic Conditions

Non-isentropic flow was produced by lowering the value of p_∞ so that a shock wave formed in the nozzle portion of the duct. For this situation the isentropic, first-order upstream boundary conditions (88) and the associated linearized solution can be used. The upstream far field quantities Q_∞ and R_∞ are constant and must be determined from the mass flow through the nozzle as explained when deriving equations (75). The mass flow can be determined by numerically integrating the mass flux crossing the downstream computational boundary each time the boundary conditions are updated.

The first-order downstream boundary condition is given by equation (109) and the associated analytic solution by equation (95). It should be noted that this solution is only an approximation to the solution of the linearized equations (23)-(25). The downstream far field quantities Q_∞ and R_∞ vary in the streamline-normal direction and can be determined from equations (76). Zero-order downstream boundary conditions as used herein consist of imposing a distribution of R_∞ along the boundary given by equations (76) with σ replaced by $1 - \frac{\gamma-1}{2} S_{\text{num}}$. This in itself represents an improvement over some applications of zero-order characteristic boundary conditions in which a constant value of the Riemann variable associated with upstream-running waves is imposed along the boundary.

Results are presented for two different values of p_∞ chosen such that a weak and a strong shock are produced in the nozzle. The strong shock spans

the width of the nozzle while the weak shock does not. Two computational boundary locations are used for each value of p_{∞} so that the accuracy of the non-isentropic boundary conditions can be evaluated.

Case 5 - Weak shock results obtained using the complete grid of Figure 3 are shown in Figures 13 and 14. Pressure and Mach number distributions are shown in Figure 13 for the centerline and lower wall. Pressure, Mach number, entropy and flow angle contours are presented in Figure 14. The non-constant Mach number in the downstream far field is evident in Figure 13. Note that the scales used in Figure 13 are much more compressed than those used for the isentropic results.

For this case, there were slight differences produced by the choice of boundary conditions, so these two sets of results are shown separately. These differences can be attributed to difficulties with the numerical fitting of a weak shock discontinuity. The shock fitting procedure is extremely sensitive to small disturbances in the numerical solution when the shock is weak, especially in the vicinity of the tail of the shock located near the center of the computational domain. These interactions were stronger when the zero-order boundary conditions were used.

Placement of the computational boundary even further downstream by using additional columns of grid cells caused very little change to the solution when the first-order boundary conditions were used, but produced noticeable differences when the zero-order conditions were used. For this reason the results of Figures 13b and 14b can be considered more accurate and can serve as a reference for evaluating the accuracy of solutions where the computational boundaries are closer to the nozzle portion of the duct.

Case 6 - Results for a shortened duct using the zero-order boundary conditions are presented in Figures 15 and 16. There were 5 columns of grid cells in both the upstream and downstream constant area portions of the duct for this case. Pressure and Mach number distributions are shown in Figure 15 and contours are shown in Figure 16. The effect of the boundary proximity is clearly evident in these results.

Case 7 - The short duct flowfield was recalculated using the first-order boundary conditions. These results are presented in Figures 17 and 18. Pressure and Mach number distributions are shown in Figure 17 and contours in Figure 18. The results agree closely with those shown in Figures 13b and 14b for the numerical solution portion of the domain. Linearized solution results obtained from equations (85) and (95) have been added upstream and downstream of the computational boundaries. Even though the solution (95) is approximate, having been obtained by linearizing the thermodynamic relation (36) and using only a two iteration approximation for the solution of equation (49), it still leads to a useful boundary condition and an adequate prediction of the downstream flowfield.

Case 8 - Strong shock results obtained using the complete grid of Figure 3 are presented in Figures 19 and 20. Pressure and Mach number distributions are shown in Figure 19 and contours in Figure 20. The significant variation of Mach number in the downstream portion of the duct is clearly evident in Figure 19. The shock fitting procedure was much less sensitive to numerical disturbances for this strong shock case. As a result, the solutions obtained using the zero-order and first-order boundary conditions for the long duct were nearly identical. These results can serve as a reference for evaluating the accuracy of solutions where the computational boundaries are closer to the nozzle portion of the duct.

Case 9 - Results for the shortened duct using the zero-order boundary conditions are presented in Figures 21 and 22. Pressure and Mach number distributions are shown in Figure 21 and contours in Figure 22. The inaccuracy of the zero-order boundary conditions for this case is evident. One noticeable effect is the change in shock position.

Case 10 - The short duct flowfield was recalculated using the first-order boundary conditions. These results are presented in Figures 23 and 24. Pressure and Mach number distributions are shown in Figure 23 and contours in Figure 24. For the numerical solution portion of the domain, the results agree closely with those shown in Figures 19 and 20. Linearized solution results obtained from Equations (85) and (95) have been added upstream and downstream of the computational boundaries. The transition across the

boundary is reasonably smooth indicating that the approximations used in developing the non-isentropic boundary conditions do not produce a strong mismatch between the numerical and analytic solutions.

Boundary Comparison - A more quantitative comparison between the zero- and first-order downstream boundary conditions can be obtained from the distribution of flow variables along the boundary. Figure 25 shows a comparison of the pressure and flow angle distributions along the downstream boundary for Cases 6 and 7 (weak shock) and Cases 9 and 10 (strong shock). Results taken from the numerical solutions of Case 5 (first-order boundary conditions) and Case 8 at the same longitudinal location are also shown. The validity of the first-order boundary condition analysis is clearly evident. The minor deviations are due in part to the approximations used in obtaining the solution (95).

For the non-isentropic calculations, 9 Fourier modes were required to give a reasonably accurate representation of the downstream boundary distributions of θ and σ for the Case 7 and 10 calculations. For the Case 5 and 8 calculations, only 7 modes were used. Implementation of the first-order boundary conditions for non-isentropic situations clearly requires more computational effort than for isentropic flow. However, this increase is warranted in view of the fact that the far field flow can contain significant streamline-normal variations in quantities other than pressure (e.g., see Figure 19).

VI. SUMMARY

Far field computational boundary conditions have been developed for 2D duct and cascade flows. These first-order boundary conditions are derived from analytic solutions of the linearized Euler equations and represent a logical extension of the zero-order (or characteristic) boundary conditions commonly used in the numerical solution of nonlinear fluid dynamic equations. The boundary conditions and analytic solutions provide a smooth transition across a computational boundary to the true far field conditions at infinity. The boundary procedure is general in that it can be used in conjunction with any numerical solution method.

For the case of isentropic flow the linearized Euler equations are solved exactly for duct and cascade flow using separation of variables and Fourier analysis. For non-isentropic flow the far field can contain significant streamline-normal variations in quantities other than pressure and flow angle, and these variations cannot be treated as small perturbations from uniform flow conditions. For the case of duct flow the non-isentropic linearized equations are solved approximately using an approximate thermodynamic relation and an iterative technique. The validity of this approximate solution has been verified by numerical results. Use of non-constant zero-order boundary conditions, which vary on the boundary as a result of entropy variations, also offer substantial improvement over constant conditions derived solely from the far field pressure. Extension of the non-isentropic analysis to cascade flows is straightforward.

Use of zero-order (or characteristic) boundary conditions requires that the computational boundaries be located far from the nonlinear region of the flow. Closer placement of the boundaries may result in a significant amount of solution degradation. The first-order boundary conditions allow the boundaries to be located much closer thereby reducing the number of grid points needed for the numerical solution and also the number of iterations for solution convergence. This allows a significant reduction in the amount of computational effort required for the nonlinear numerical solution because the

additional calculations required for the first-order boundary conditions is modest.

The boundary condition procedures developed herein can be extended to axisymmetric, three-dimensional, and viscous flows, including external flows. It is recommended that these analyses be undertaken and also that the present results be extended to non-isentropic cascade flows.

Acknowledgement - This work was partially supported by Naval Air System Command (G. Derderian - Program Manager) under contracts N62271-84-M-1857 and N62271-86-M-0202, from the Naval Postgraduate School, Monterey, Ca., where the technical monitor was Professor Raymond P. Shreeve.

The author would also like to thank Mr. David S. Stookesberry for his help in performing the computations.

VII. REFERENCES

1. Verhoff, A. and O'Neil, P. J., "A Natural Formulation for Numerical Solution of the Euler Equations," AIAA Paper No. 84-0163 Jan. 1984.
2. Verhoff, A., "Modeling of Computational and Solid Surface Boundary Conditions for Fluid Dynamics Calculations," AIAA Paper No. 85-1496 CP, July 1985.
3. Hirsch, Ch., and Verhoff, A., "Far Field Numerical Boundary Conditions for Internal and Cascade Flow Computations," AIAA Paper, To Be Published, 1989.
4. Moretti, G., "A Technique for Integrating Two-Dimensional Euler Equations," Computers and Fluids, Vol. 15, No. 1, March 1987, pg. 59-75.

III. APPENDIX A: EVALUATION OF INTEGRALS

Evaluation of the integrals appearing in equations (96), (97), (98) and (100) will be presented here. They are defined as shown below.

Equation (96):

$$I_1 = \frac{1}{n\pi} \int_0^y \phi_n \cos n\pi(y-\eta) d\eta$$

Equation (97):

$$I_2 = \frac{1}{n\pi} \int_0^y \phi_n \sin n\pi(y-\eta) d\eta$$

Equation (98):

$$I_3 = \frac{1}{n\pi\beta A_n} \int_0^1 \phi_n \sin n\pi y dy$$

Equation (100):

$$I_4 = \int_0^1 \sin m\pi y \cos n\pi y y dy$$

$$I_5 = \int_0^1 \sin m\pi y \int_0^y \phi_n \sin n\pi(\eta-y) d\eta dy$$

The quantity ϕ_n appearing in the integrands is defined by equation (94).

Evaluation of I₁

$$\begin{aligned}
 I_1 &= \frac{1}{\gamma-1} \frac{A_n}{\beta^2 q_\infty^2} \left\{ \sum_{k=1}^{\infty} \left(k - \frac{1}{2}\right) D_k \left[\frac{\sin(n+k-1/2)\pi y + \sin n\pi y}{2n+k-1/2} \right. \right. \\
 &\quad \left. \left. + \frac{\sin(n-k+1/2)\pi y + \sin n\pi y}{2n-k+1/2} + \frac{\sin(n+k-1/2)\pi y - \sin(n-k+1/2)\pi y}{k-1/2} \right] \right. \\
 &\quad \left. + n \bar{M}_\infty^2 \sum_{k=1}^{\infty} D_k \left[\frac{\sin(n+k-1/2)\pi y + \sin n\pi y}{2n+k-1/2} - \frac{\sin(n-k+1/2)\pi y + \sin n\pi y}{2n-k+1/2} \right. \right. \\
 &\quad \left. \left. + \frac{\sin(n+k-1/2)\pi y + \sin(n-k+1/2)\pi y - 2\sin n\pi y}{k-1/2} \right] - 2\bar{M}_\infty^2 \sigma_w n\pi y \sin n\pi y \right\}
 \end{aligned}$$

Evaluation of I₂

$$\begin{aligned}
 I_2 &= \frac{1}{\gamma-1} \frac{A_n}{\beta^2 q_\infty^2} \left\{ \sum_{k=1}^{\infty} \left(k - \frac{1}{2}\right) D_k \left[\frac{\cos(n+k-1/2)\pi y - \cos n\pi y}{2n+k-1/2} \right. \right. \\
 &\quad \left. \left. + \frac{\cos(n-k+1/2)\pi y - \cos n\pi y}{2n-k+1/2} + \frac{\cos(n-k+1/2)\pi y - \cos(n+k-1/2)\pi y}{k-1/2} \right] \right. \\
 &\quad \left. + n \bar{M}_\infty^2 \sum_{k=1}^{\infty} D_k \left[\frac{\cos(n+k-1/2)\pi y - \cos n\pi y}{2n+k-1/2} - \frac{\cos(n-k+1/2)\pi y - \cos n\pi y}{2n-k+1/2} \right. \right. \\
 &\quad \left. \left. - \frac{\cos(n+k-1/2)\pi y + \cos(n-k+1/2)\pi y - 2\cos n\pi y}{k-1/2} \right] \right. \\
 &\quad \left. - 2\bar{M}_\infty^2 \sigma_w [\sin n\pi y - n\pi y \cos n\pi y] \right\}
 \end{aligned}$$

Evaluation of I₃

$$\begin{aligned}
 I_3 &= \frac{1}{\gamma-1} \frac{1}{\beta^3 q_\infty^2} \left\{ \sum_{k=1}^{\infty} \left(k - \frac{1}{2}\right) D_k \left[\frac{1}{2n+k-1/2} + \frac{1}{2n-k+1/2} \right] \right. \\
 &\quad \left. + n \bar{M}_\infty^2 \sum_{k=1}^{\infty} D_k \left[\frac{1}{2n+k-1/2} - \frac{1}{2n-k+1/2} - \frac{2}{k-1/2} \right] - 2\pi \bar{M}_\infty^2 n \sigma_w \right\}
 \end{aligned}$$

Evaluation of I₄

$$I_4 = \begin{cases} -\frac{1}{4\pi m} & ; & n=m \\ -\frac{(-1)^{m+n}}{\pi} \frac{m}{m^2-n^2} & ; & n \neq m \end{cases}$$

Evaluation of I₅

$$I_5 = \begin{cases} -\frac{1}{2} \beta A_m \delta \lambda_m - \frac{1}{2} \int_0^1 (1-y) \phi_m \cos m\pi y \, dy & ; & n=m \\ \frac{n}{m^2-n^2} \left[\frac{1}{\pi} \int_0^1 \phi_n \sin m\pi y \, dy - (-1)^{m+n} \beta m A_n \delta \lambda_n \right] & ; & n \neq m \end{cases}$$

$$\int_0^1 (1-y) \phi_m \cos m\pi y \, dy = \frac{1}{\gamma-1} \frac{mA_m}{\beta^2 q_\infty^2} \left\{ \sum_{k=1}^{\infty} \left(k-\frac{1}{2}\right) D_k \left[\frac{1}{(2m+k-1/2)^2} + \frac{1}{(2m-k+1/2)^2} + \frac{2}{(k-1/2)^2} \right] + m \bar{M}_\infty^2 \sum_{k=1}^{\infty} D_k \left[\frac{1}{(2m+k-1/2)^2} - \frac{1}{(2m-k+1/2)^2} \right] - \pi \sigma_w \bar{M}_\infty^2 \right\}$$

$$\int_0^1 \phi_n \sin m\pi y \, dy = \frac{\pi}{\gamma-1} \frac{nA_n}{\beta^2 q_\infty^2} \left\{ \sum_{k=1}^{\infty} \left(k-\frac{1}{2}\right) D_k \left[\frac{1}{m+n+k-1/2} + \frac{1}{m-n-k+1/2} + \frac{1}{m+n-k+1/2} + \frac{1}{m-n+k-1/2} \right] + n \bar{M}_\infty^2 \sum_{k=1}^{\infty} D_k \left[\frac{1}{m+n+k-1/2} + \frac{1}{m-n-k+1/2} - \frac{1}{m+n-k+1/2} - \frac{1}{m-n+k-1/2} \right] \right\}$$

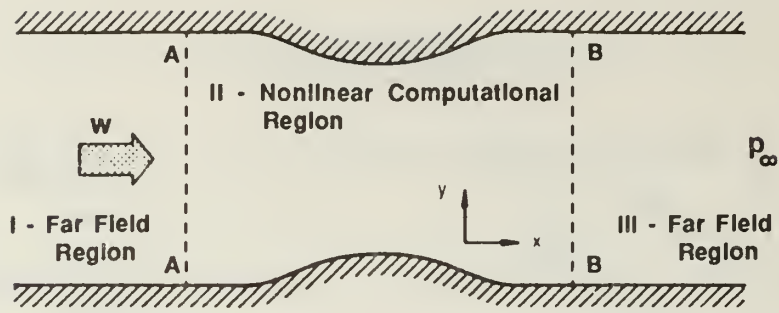


Figure 1. Duct/Nozzle Schematic

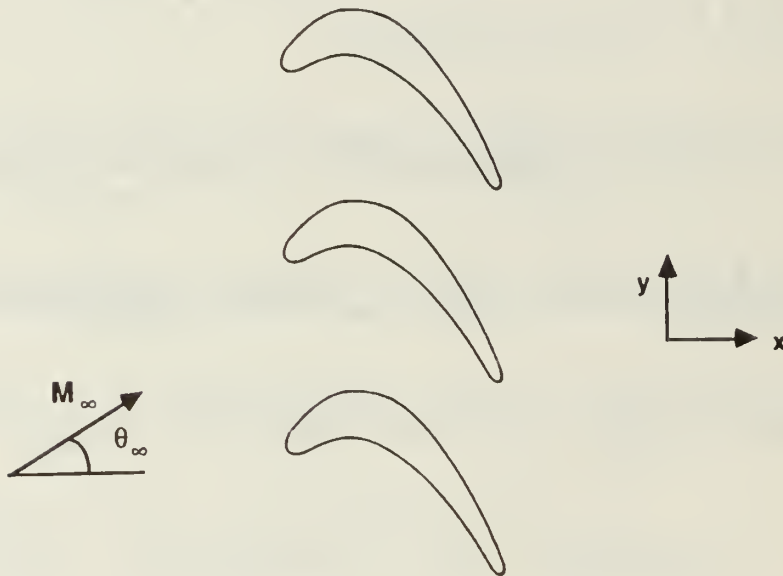


Figure 2. Cascade Schematic

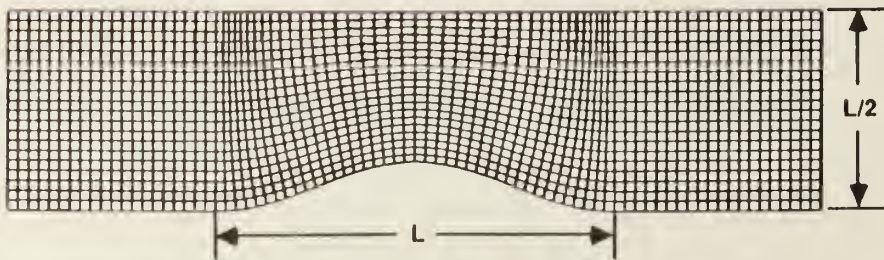
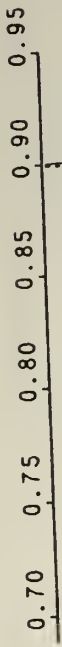


Figure 3. Duct/Nozzle Geometry and Grid

Pressure



Mach Number



— Surface
- - - Centerline

Computational Grid (81x21)

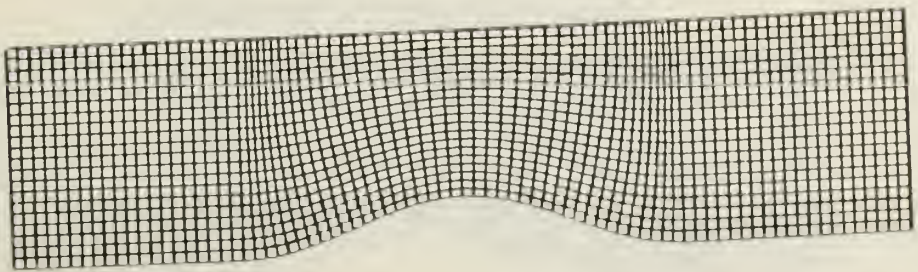
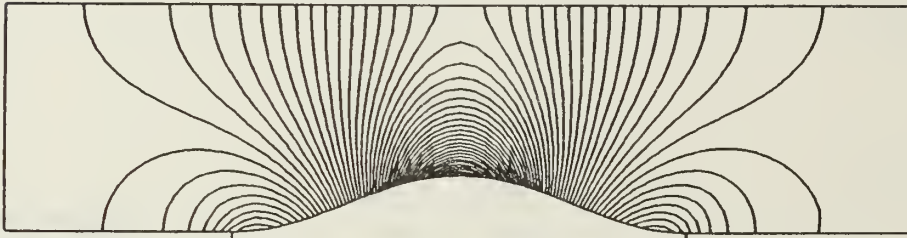


Figure 4. Pressure and Mach Number Distributions
Zero- and First-Order Boundary Conditions
 $p_{\infty} = 0.90$

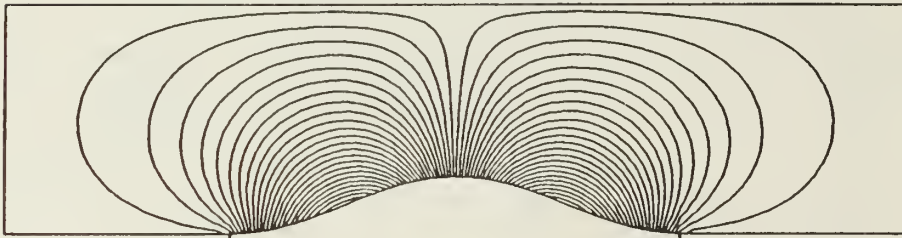
Pressure Contours



Mach Number Contours



Flow Angle Contours



Computational Grid (81x21)

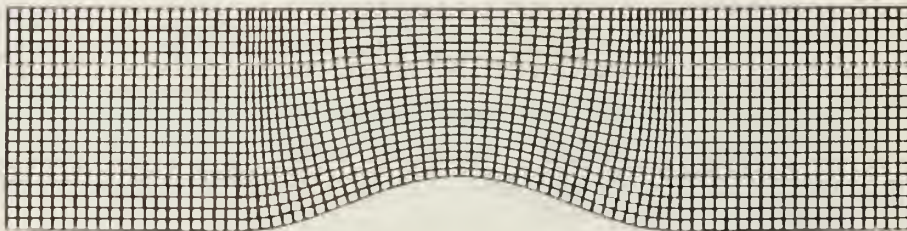
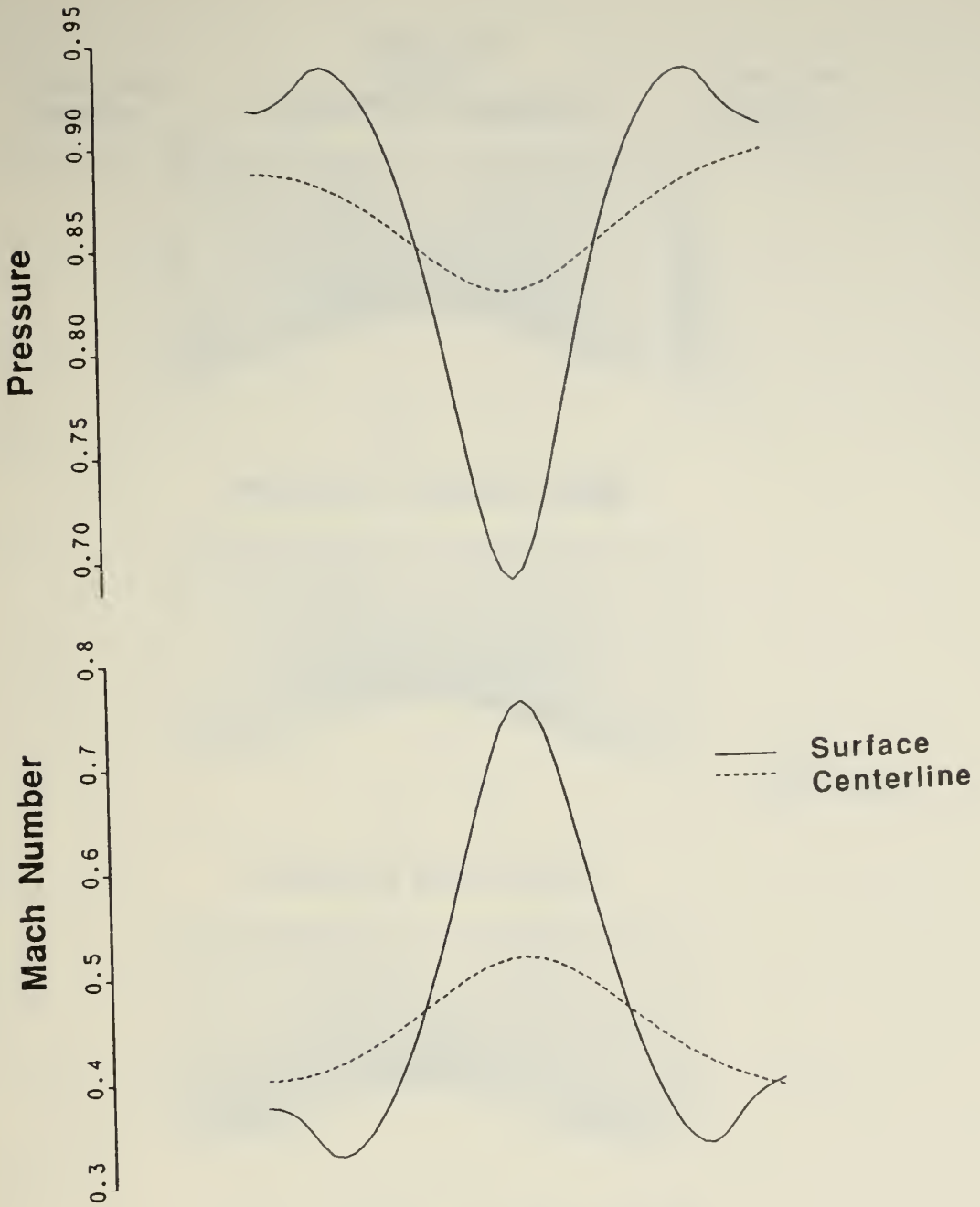


Figure 5. Pressure, Mach Number and Flow Angle Contours
Zero- and First-Order Boundary Conditions
 $p_{\infty} = 0.90$



Computational Grid (51x21)

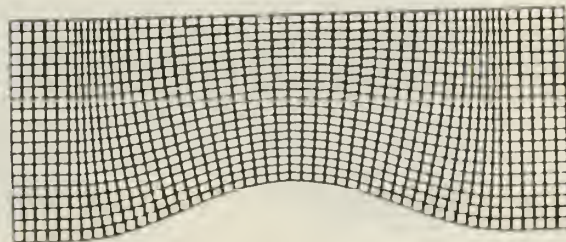
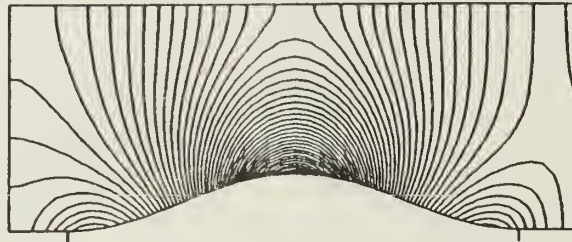


Figure 6. Pressure and Mach Number Distributions
 Zero-Order Boundary Conditions
 $p_{\infty} = 0.90$

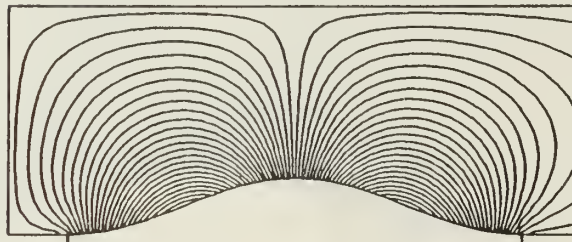
Pressure Contours



Mach Number Contours



Flow Angle Contours



Computational Grid (51x21)

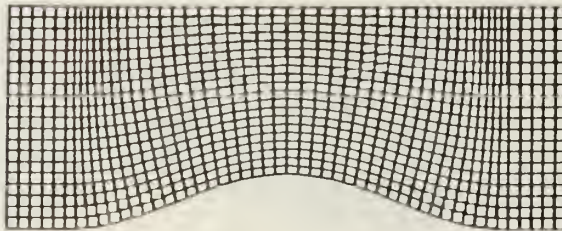


Figure 7. Pressure, Mach Number and Flow Angle Contours
Zero-Order Boundary Conditions
 $p_{\infty} = 0.90$

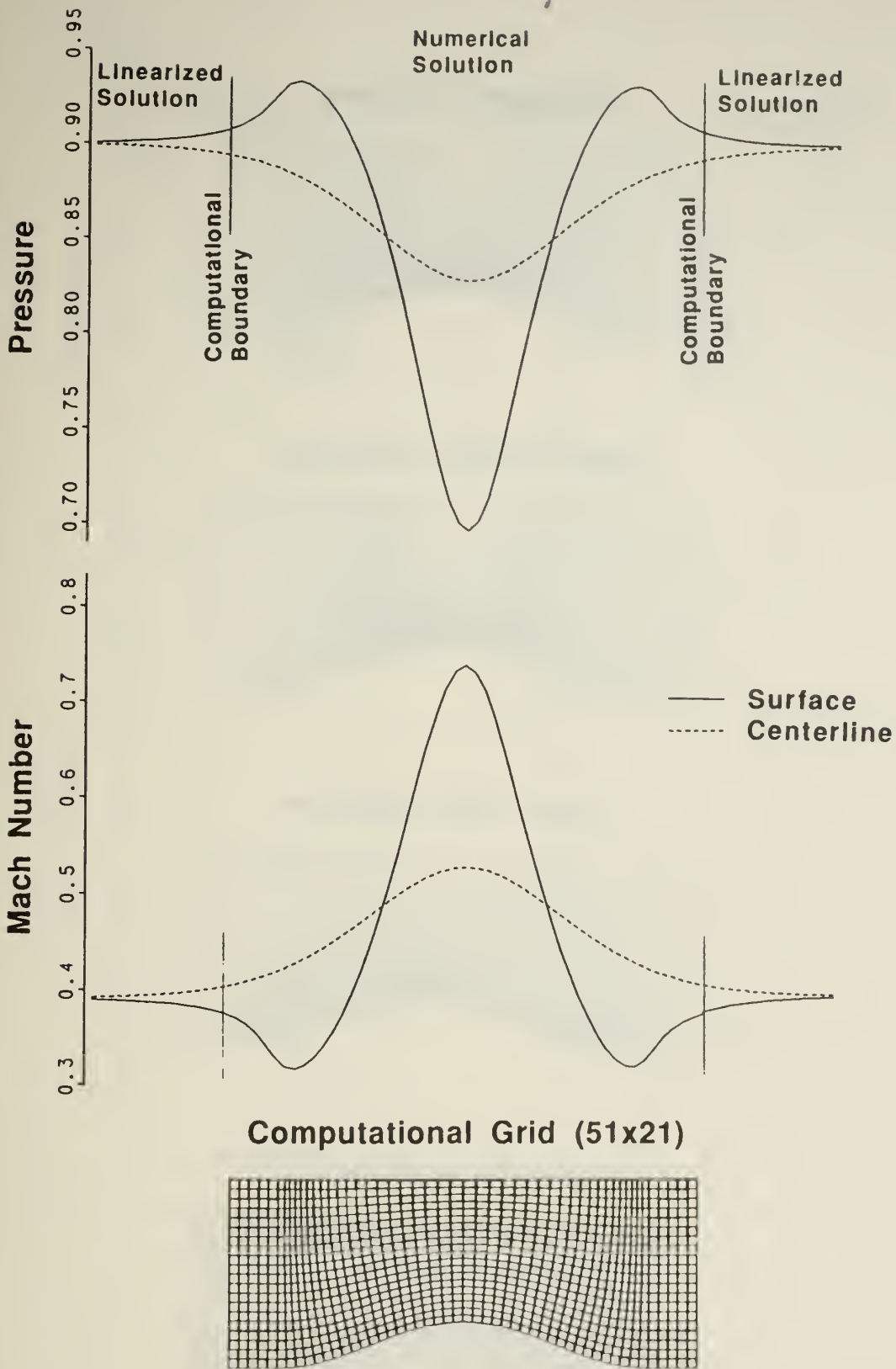
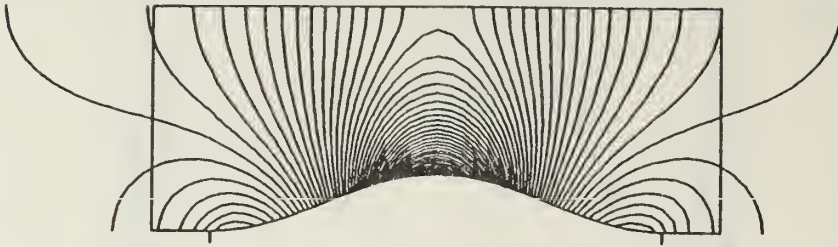
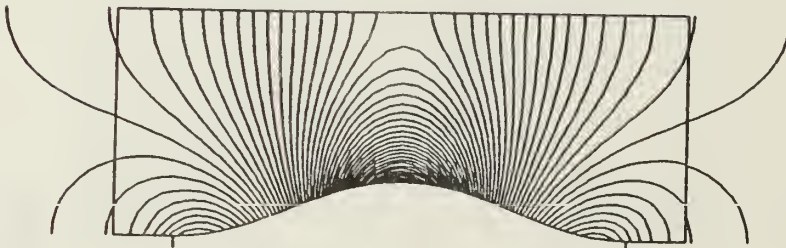


Figure 8. Pressure and Mach Number Distributions
 First-Order Boundary Conditions
 $p_{\infty} = 0.90$

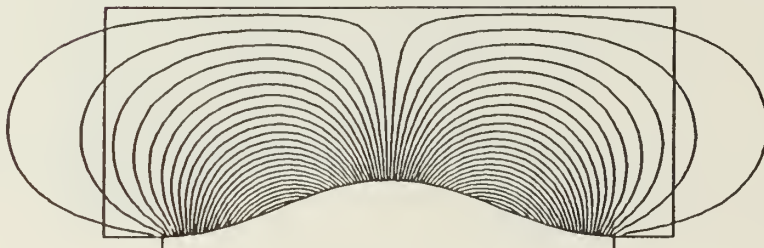
Pressure Contours



Mach Number Contours



Flow Angle Contours



Computational Grid (51x21)

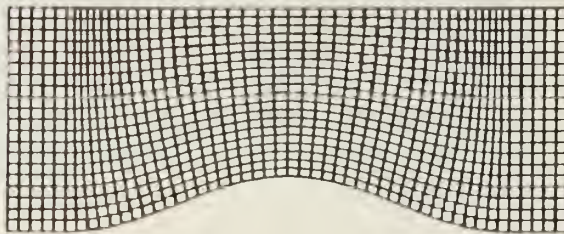
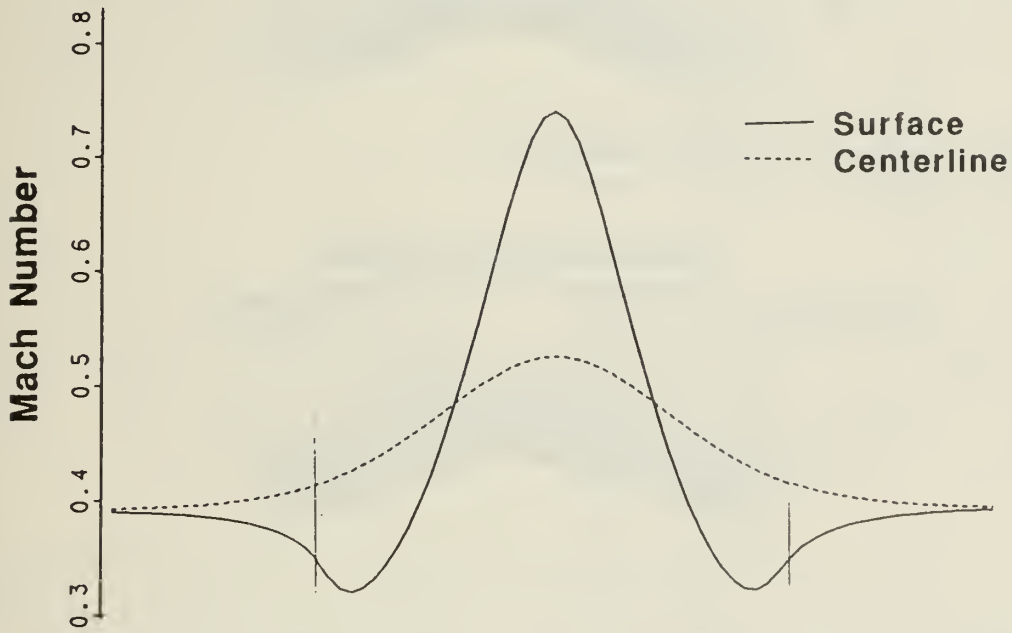
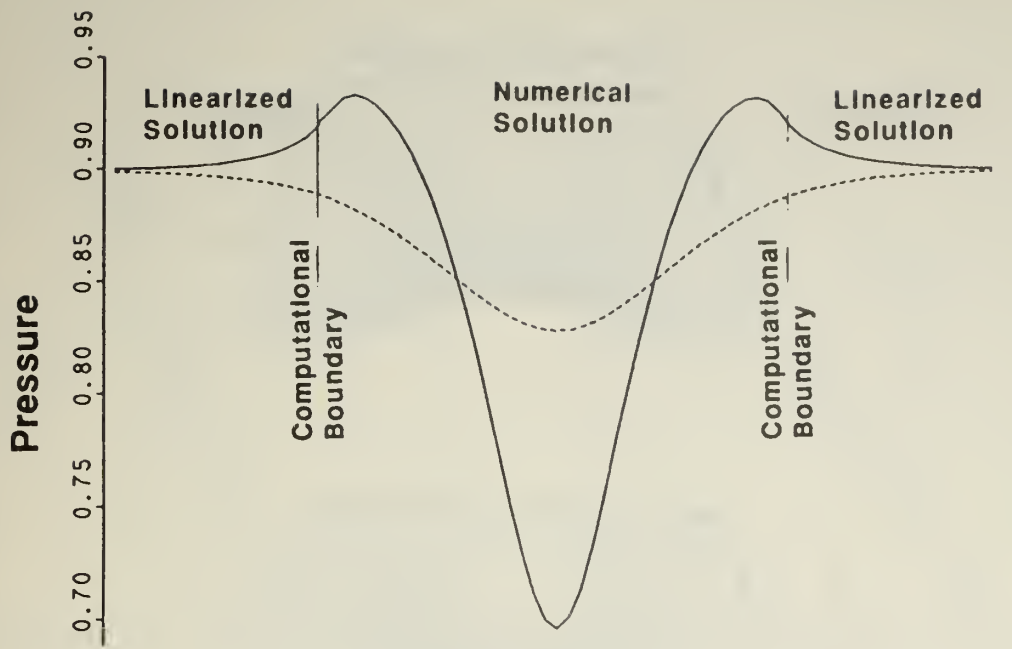


Figure 9. Pressure, Mach Number and Flow Angle Contours
First-Order Boundary Conditions
 $p_{\infty} = 0.90$



Computational Grid (43x21)

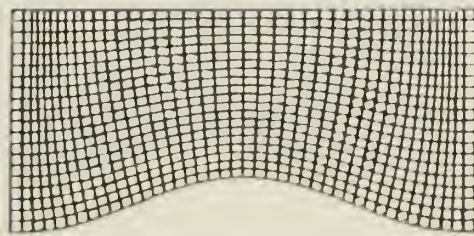
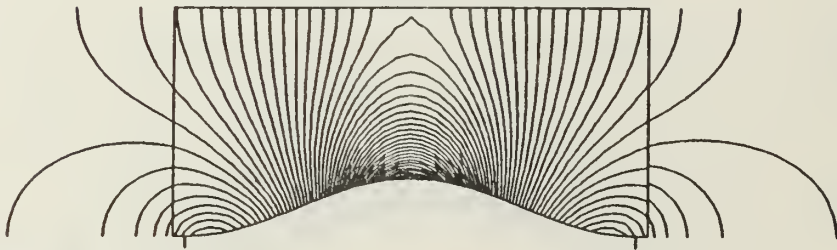


Figure 10. Pressure and Mach Number Distributions
 First-Order Boundary Conditions
 $p_{\infty} = 0.90$

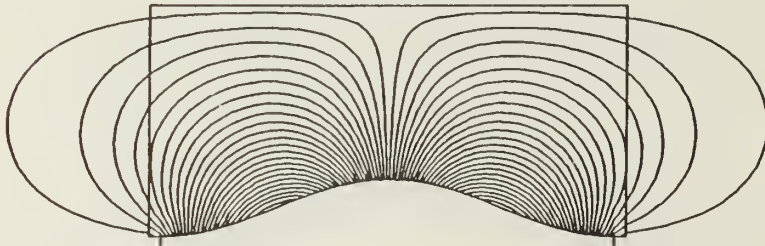
Pressure Contours



Mach Number Contours



Flow Angle Contours



Computational Grid (43x21)

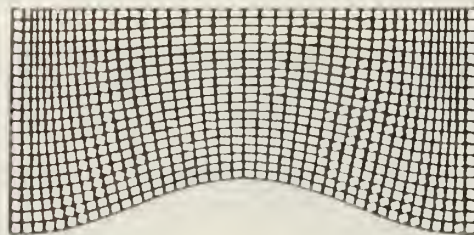
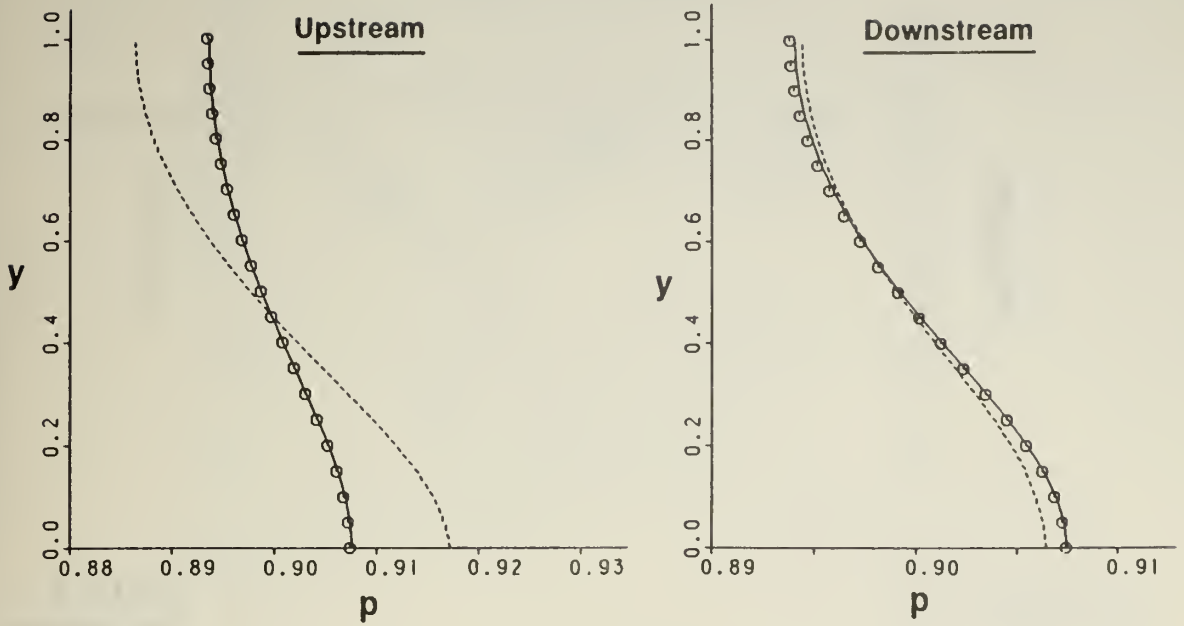


Figure 11. Pressure, Mach Number and Flow Angle Contours
First-Order Boundary Conditions
 $p_{\infty} = 0.90$

Pressure Distribution



- Numerical Solution (Case 1)
- - - Zero-Order Boundary Conditions (Case 2)
- First-Order Boundary Conditions (Case 3)

Flow Angle Distribution

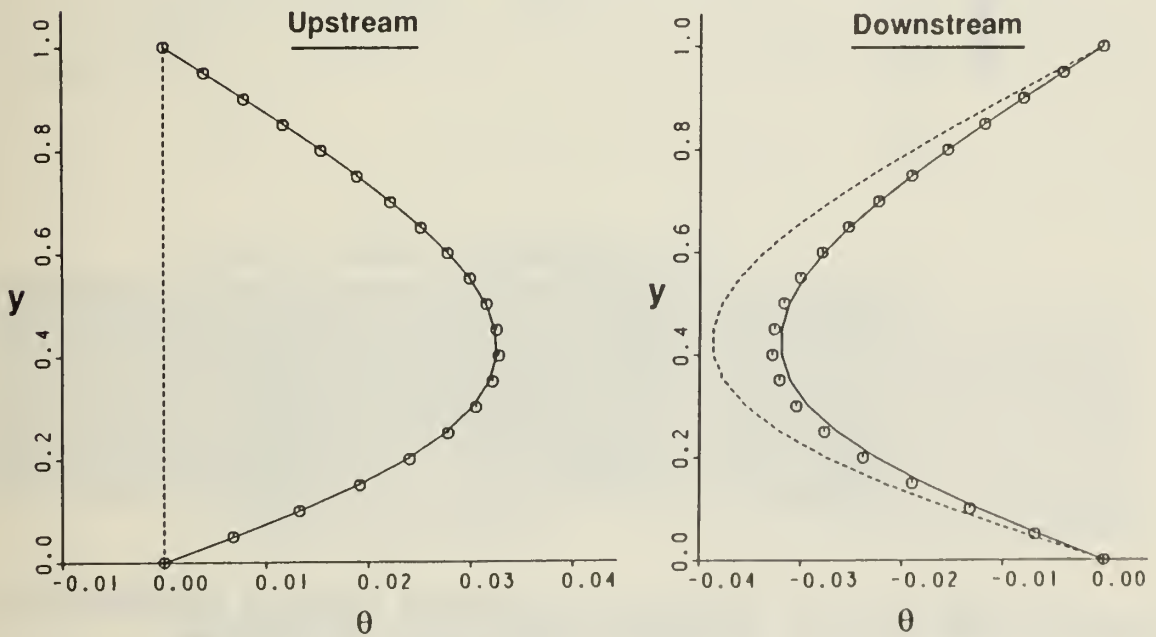


Figure 12. Pressure and Flow Angle Distributions on Computational Boundaries
 $p_{\infty} = 0.90$

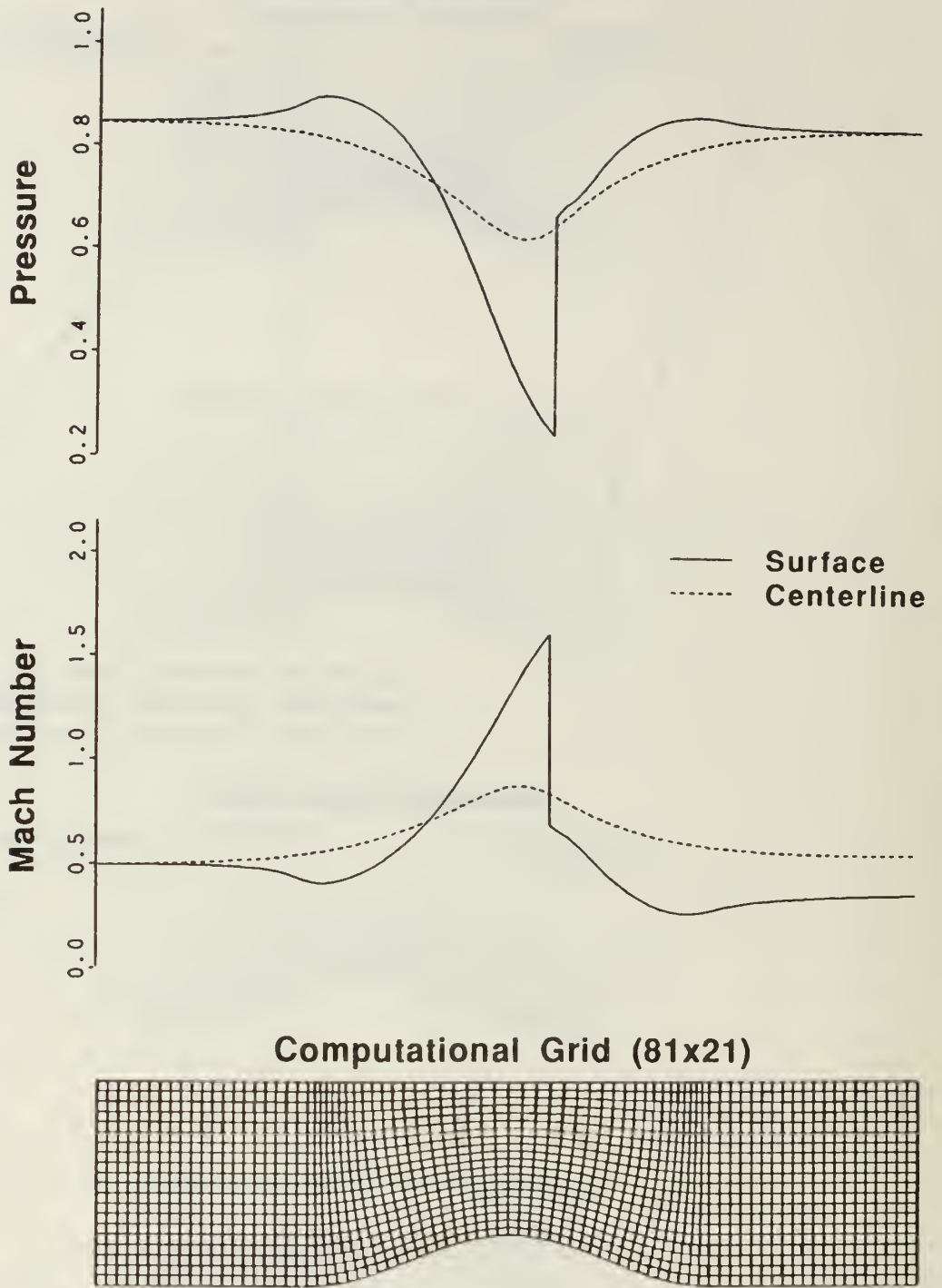
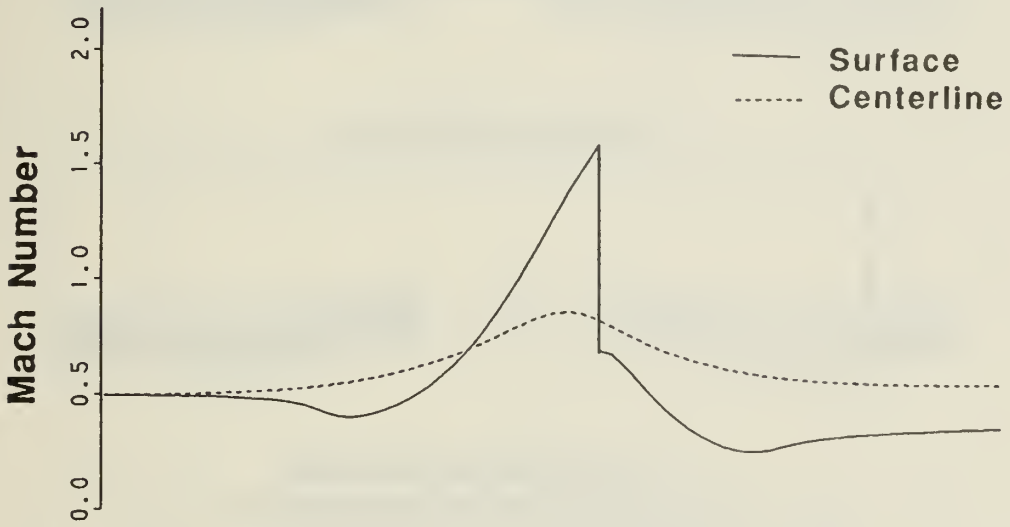
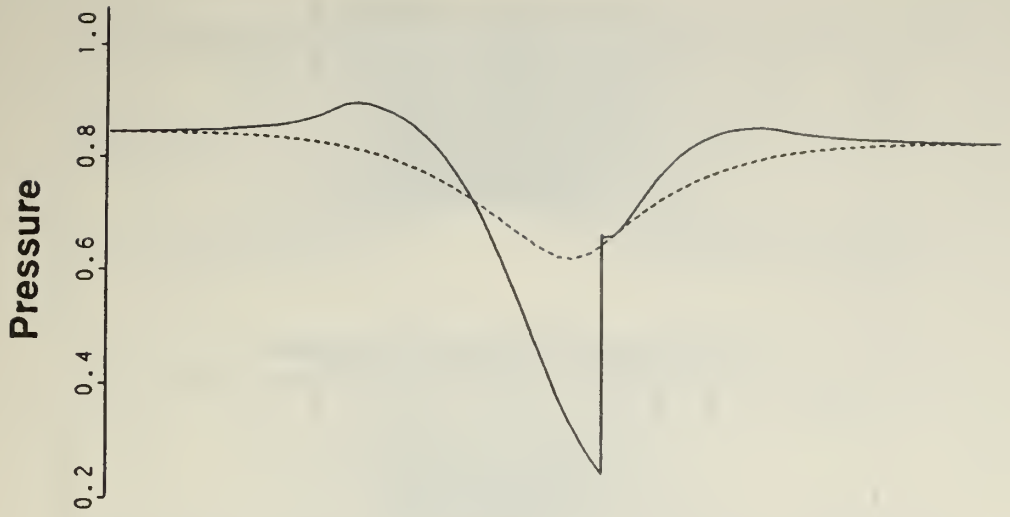


Figure 13a. Pressure and Mach Number Distributions
 Zero-Order Boundary Conditions
 $p_\infty = 0.83$



Computational Grid (81x21)

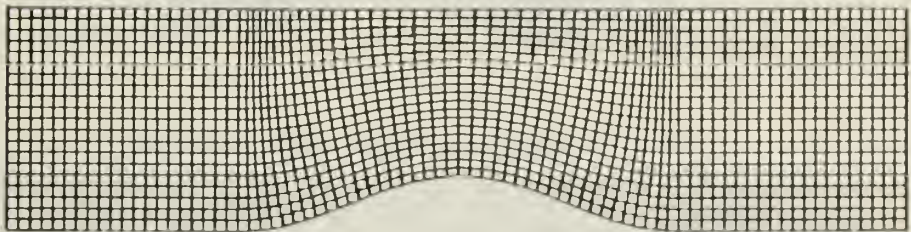
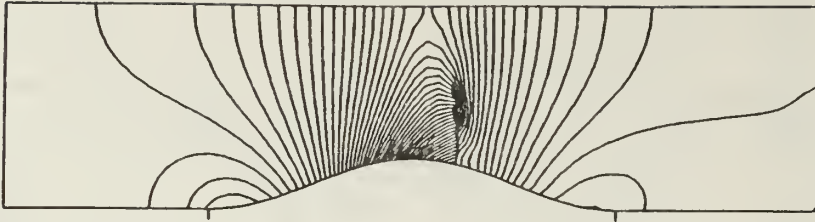
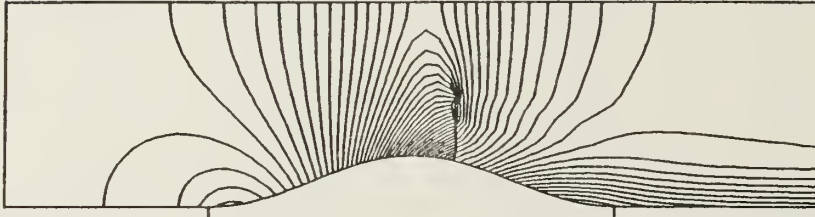


Figure 13b. Pressure and Mach Number Distributions
 First-Order Boundary Conditions
 $p_{\infty} = 0.83$

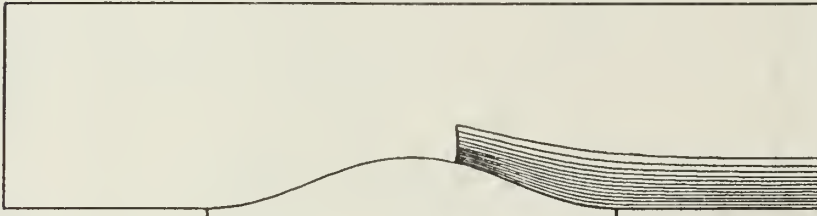
Pressure Contours



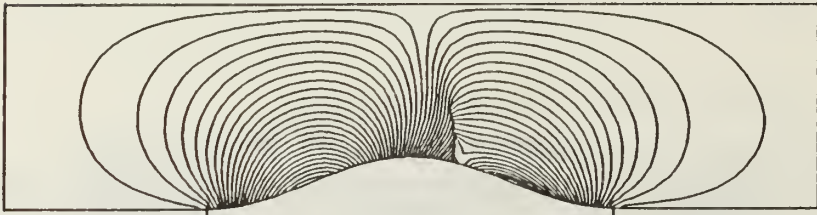
Mach Number Contours



Entropy Contours



Flow Angle Contours



Computational Grid (81x21)

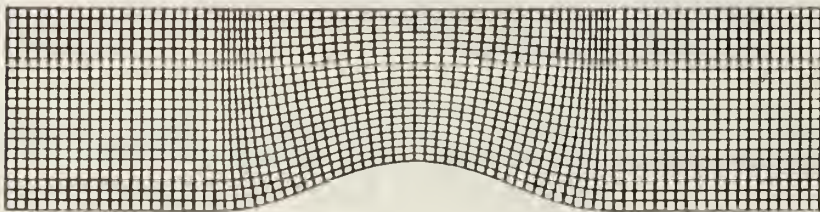
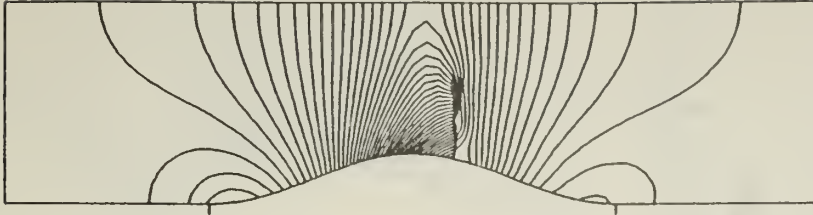
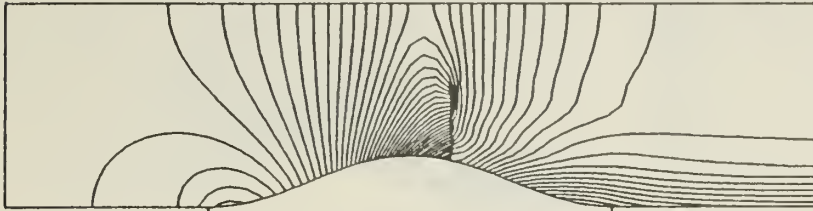


**Figure 14a. Pressure, Mach Number, Entropy and Flow Angle Contours
Zero-Order Boundary Conditions
 $p_{\infty} = 0.83$**

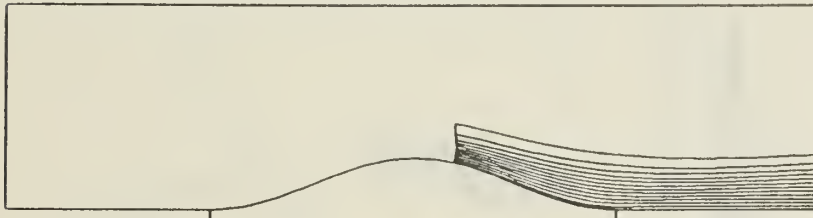
Pressure Contours



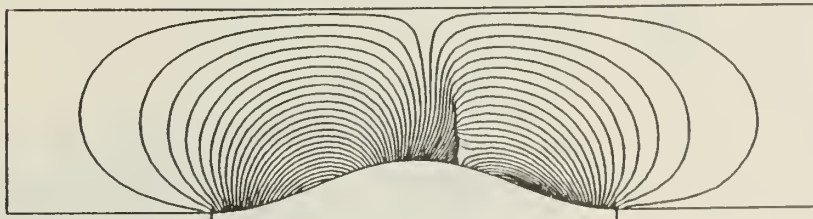
Mach Number Contours



Entropy Contours



Flow Angle Contours



Computational Grid (81x21)

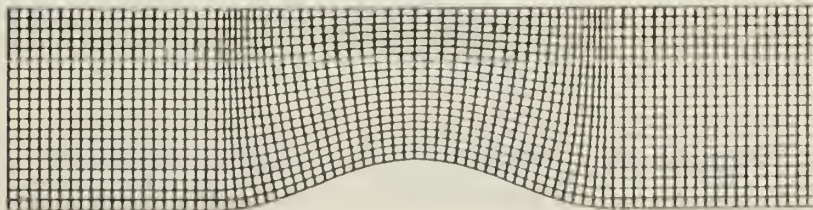


Figure 14b. Pressure, Mach Number, Entropy and Flow Angle Contours
First-Order Boundary Conditions
 $p_{\infty} = 0.83$

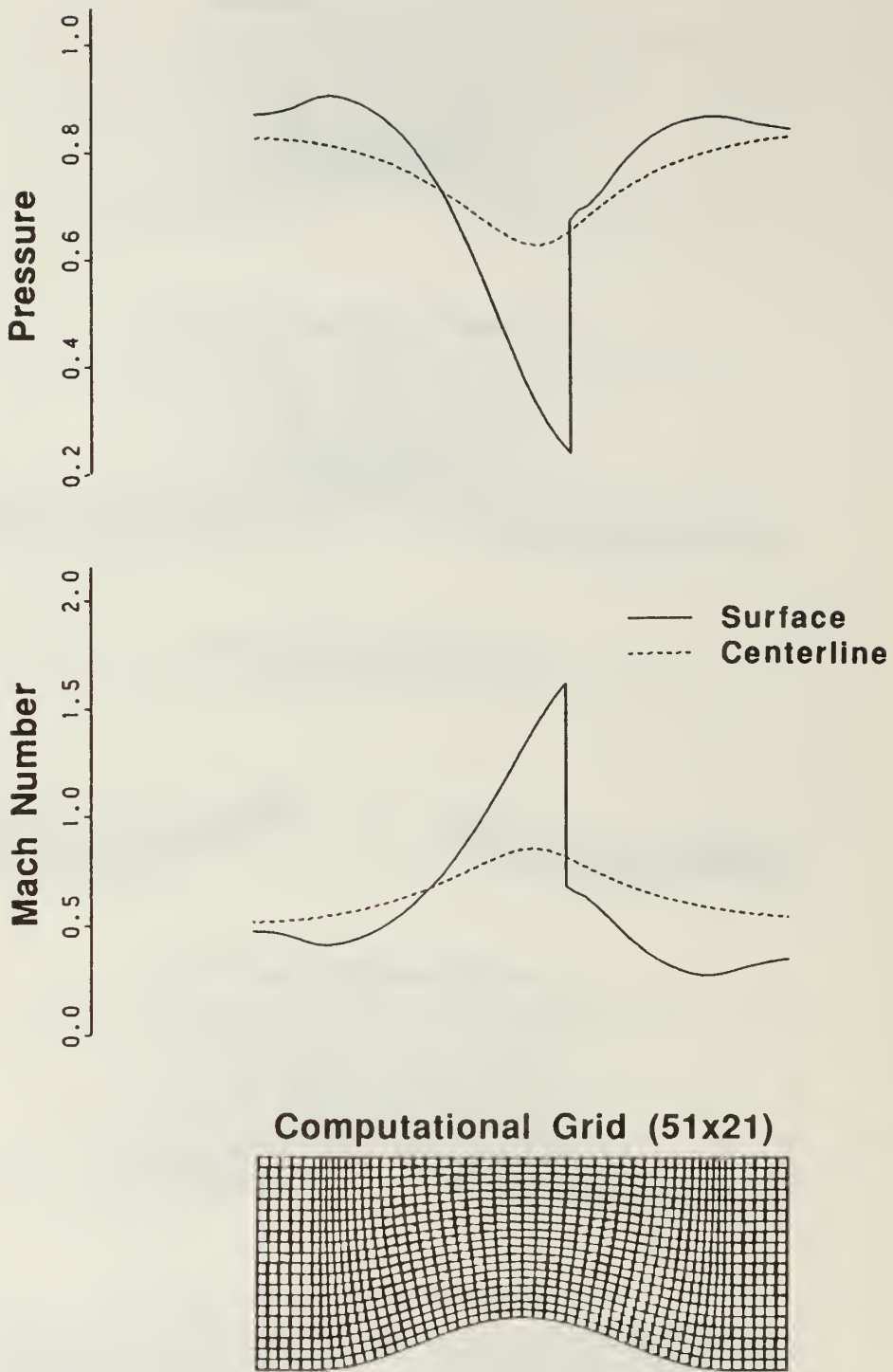
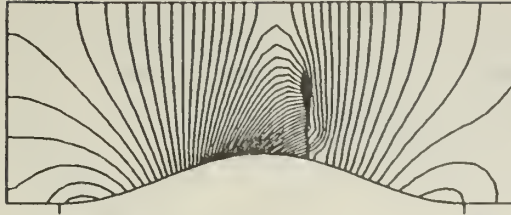
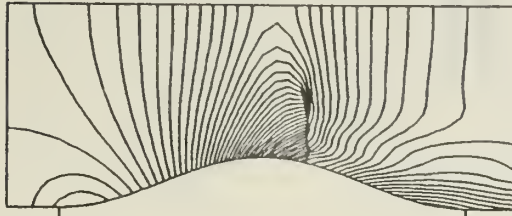


Figure 15. Pressure and Mach Number Distributions
 Zero-Order Boundary Conditions
 $p_{\infty} = 0.83$

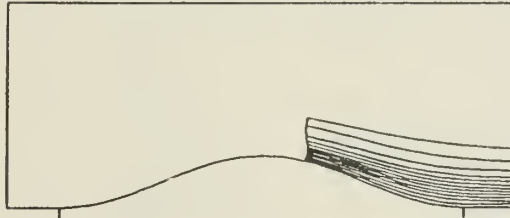
Pressure Contours



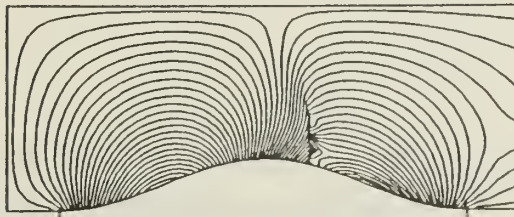
Mach Number Contours



Entropy Contours



Flow Angle Contours



Computational Grid (51x21)

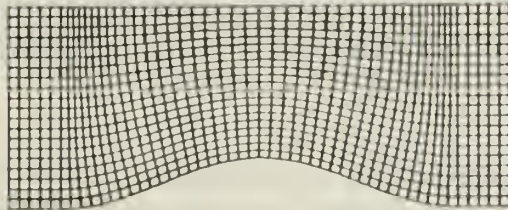


Figure 16. Pressure, Mach Number, Entropy and Flow Angle Contours
Zero-Order Boundary Conditions
 $p_{\infty} = 0.83$

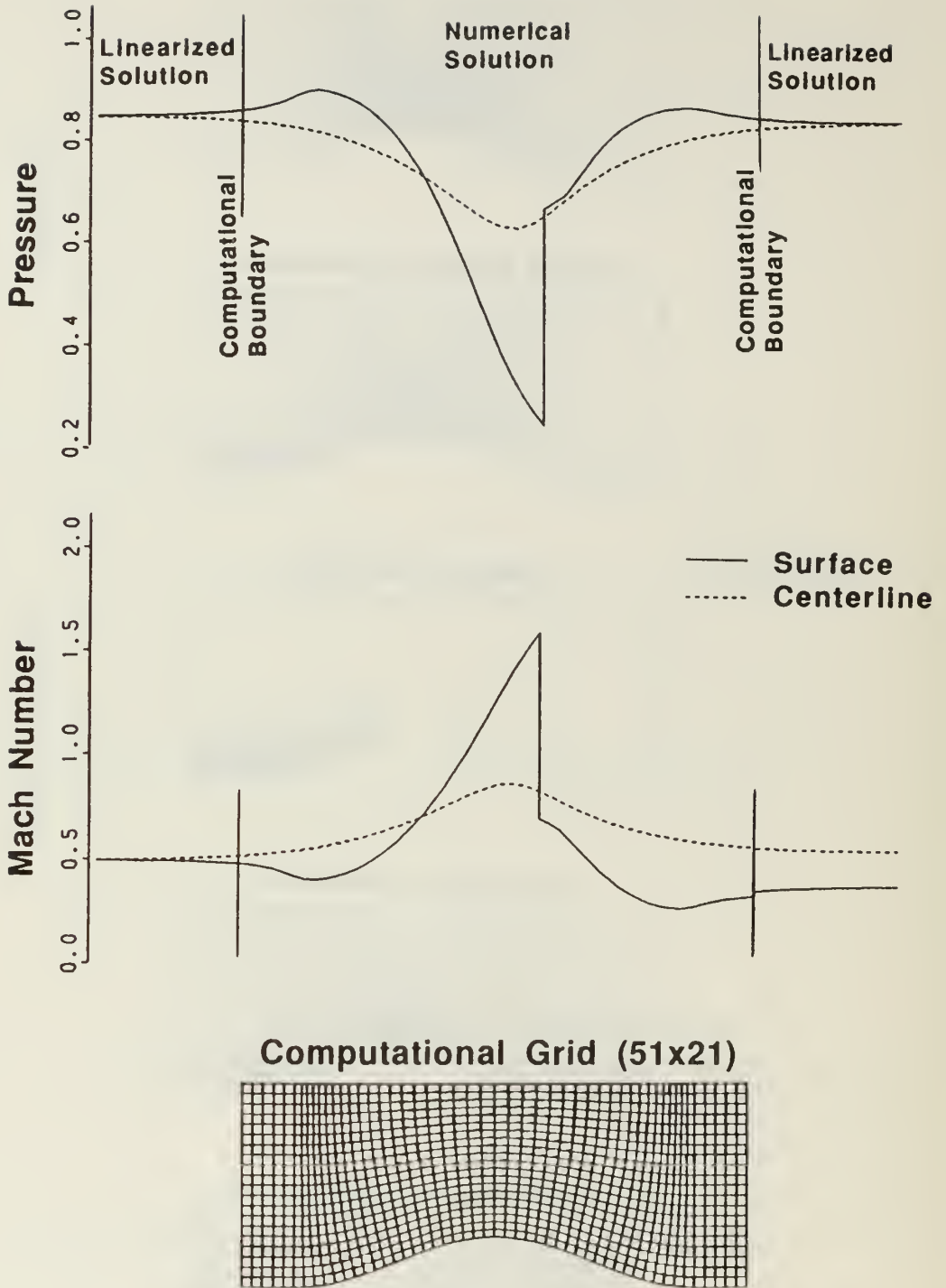
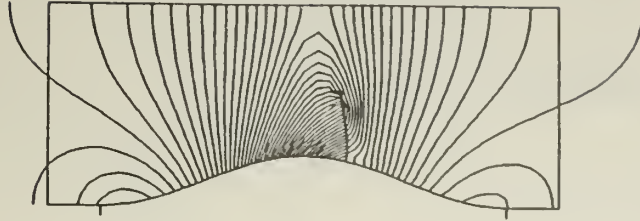
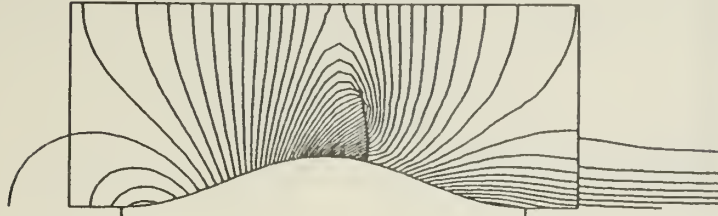


Figure 17. Pressure and Mach Number Distributions
 First-Order Boundary Conditions
 $p_{\infty} = 0.83$

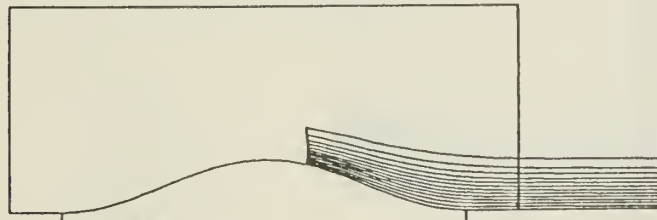
Pressure Contours



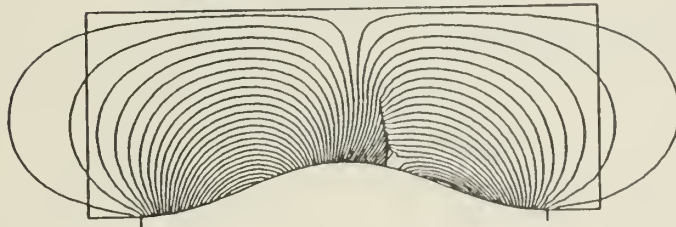
Mach Number Contours



Entropy Contours



Flow Angle Contours



Computational Grid (51x21)

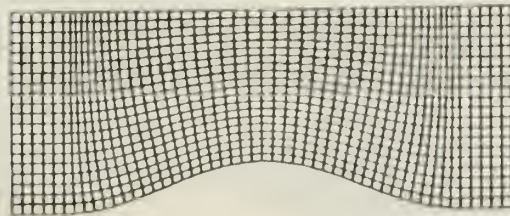
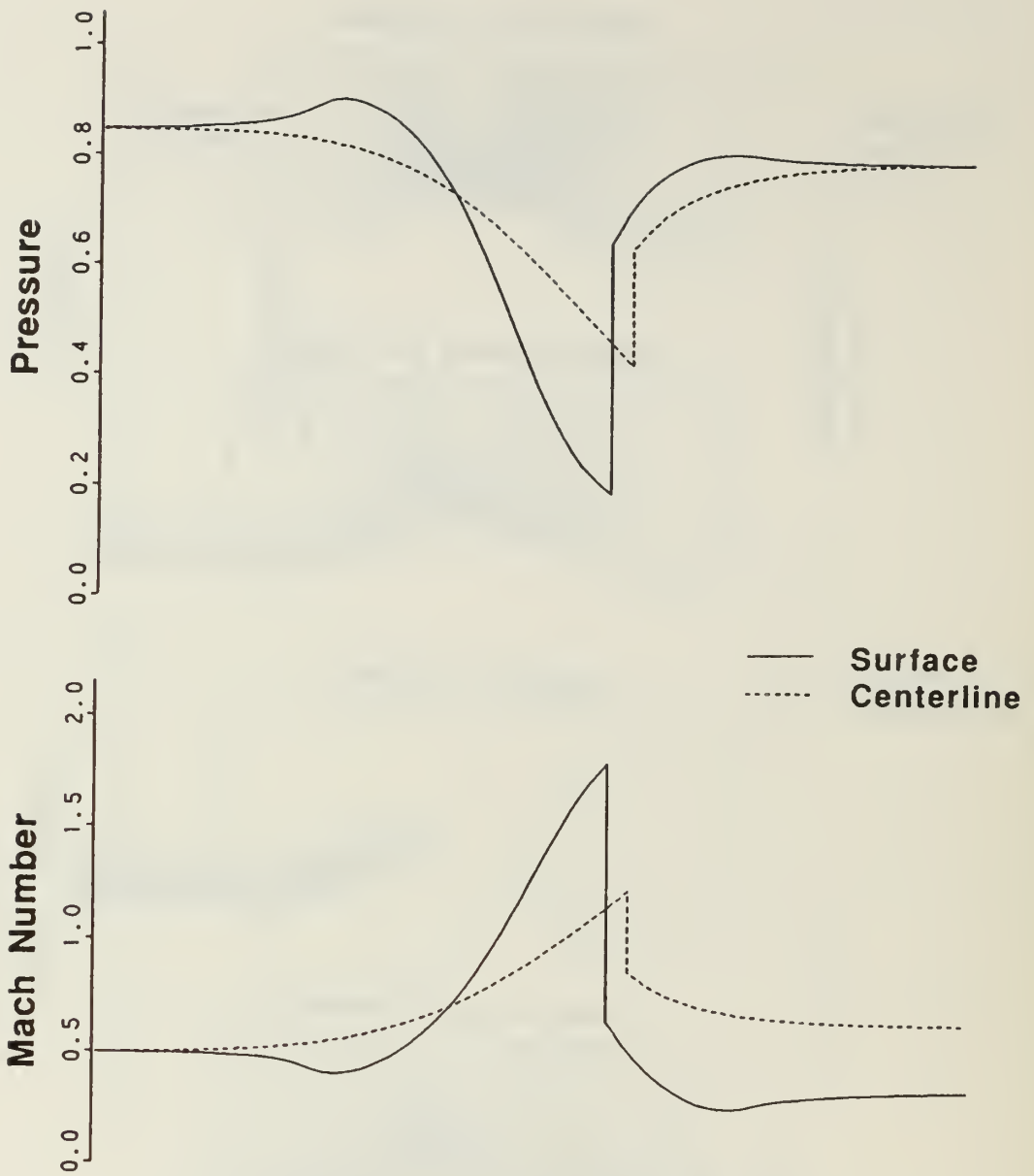


**Figure 18. Pressure, Mach Number, Entropy and Flow Angle Contours
First-Order Boundary Conditions
 $p_{\infty} = 0.83$**



Computational Grid (81x21)

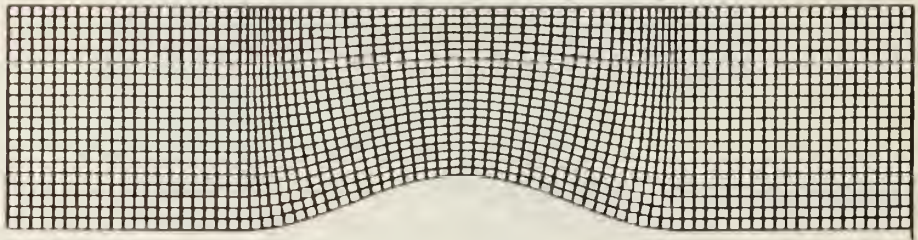
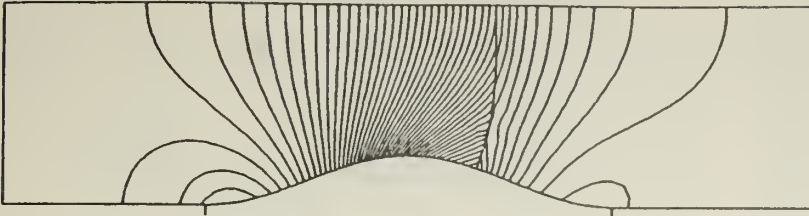
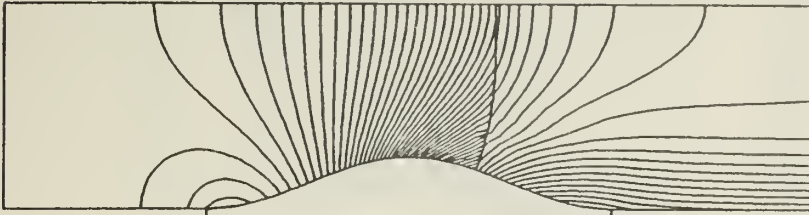


Figure 19. Pressure and Mach Number Distributions
 Zero- and First-Order Boundary Conditions
 $p_{\infty} = 0.78$

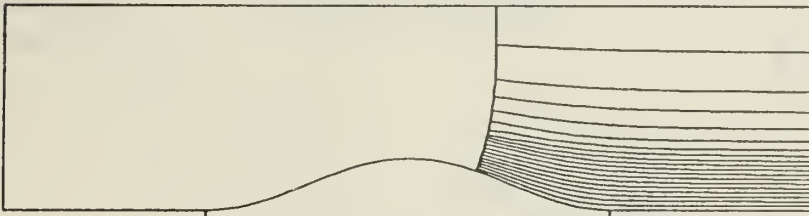
Pressure Contours



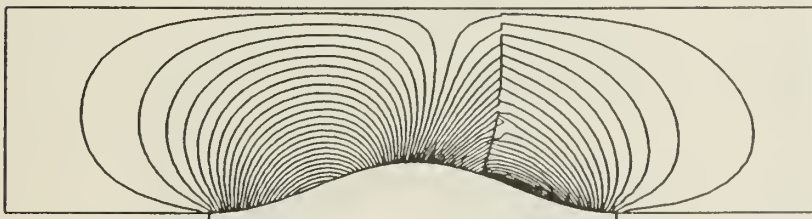
Mach Number Contours



Entropy Contours



Flow Angle Contours



Computational Grid (81x21)

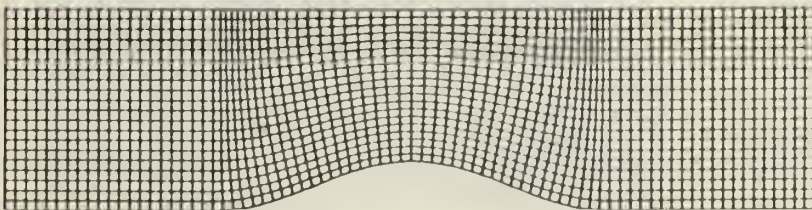
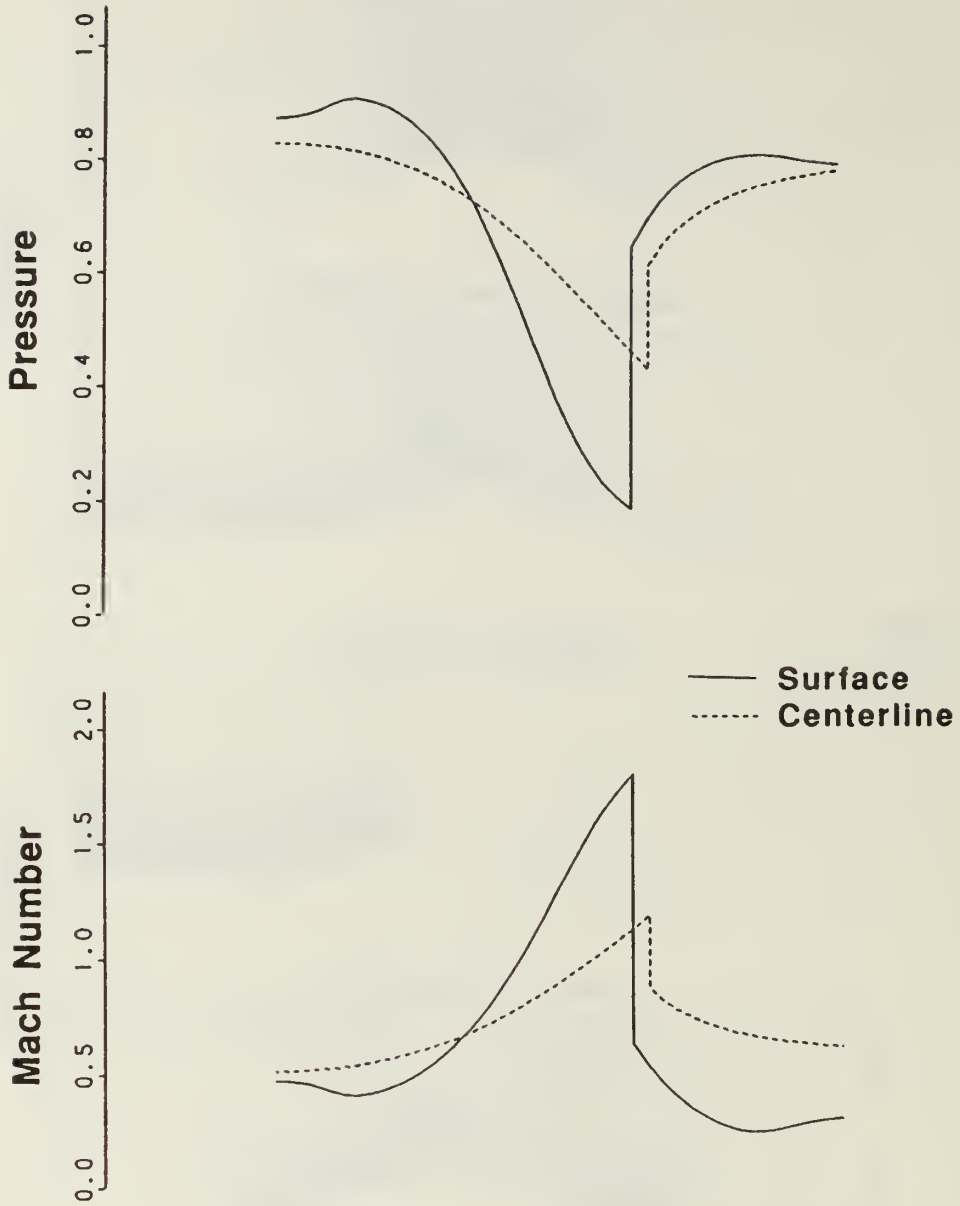
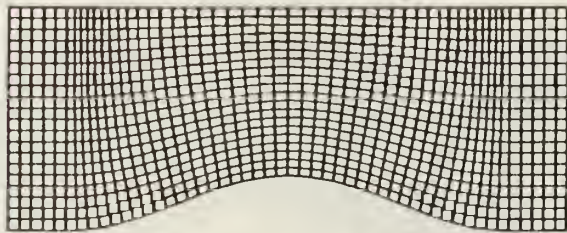


Figure 20. Pressure, Mach Number, Entropy and Flow Angle Contours
Zero- and First-Order Boundary Conditions
 $p_{\infty} = 0.78$

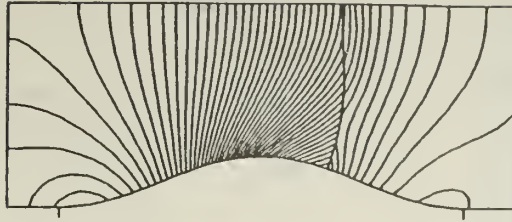


Computational Grid (51x21)

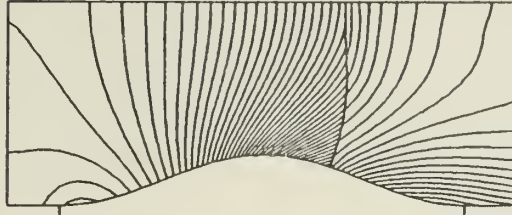


**Figure 21. Pressure and Mach Number Distributions
Zero-Order Boundary Conditions
 $p_{\infty} = 0.78$**

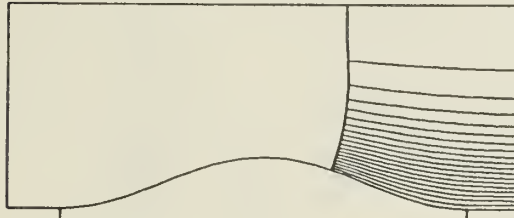
Pressure Contours



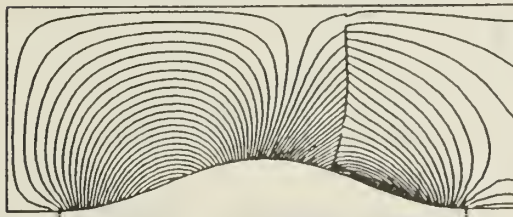
Mach Number Contours



Entropy Contours



Flow Angle Contours



Computational Grid (51x21)

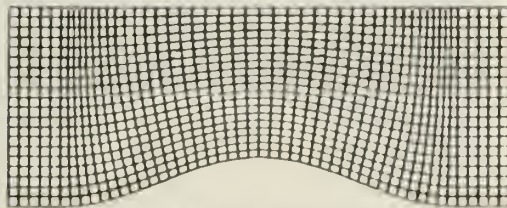


Figure 22. Pressure, Mach Number, Entropy and Flow Angle Contours
Zero-Order Boundary Conditions
 $p_{\infty} = 0.78$

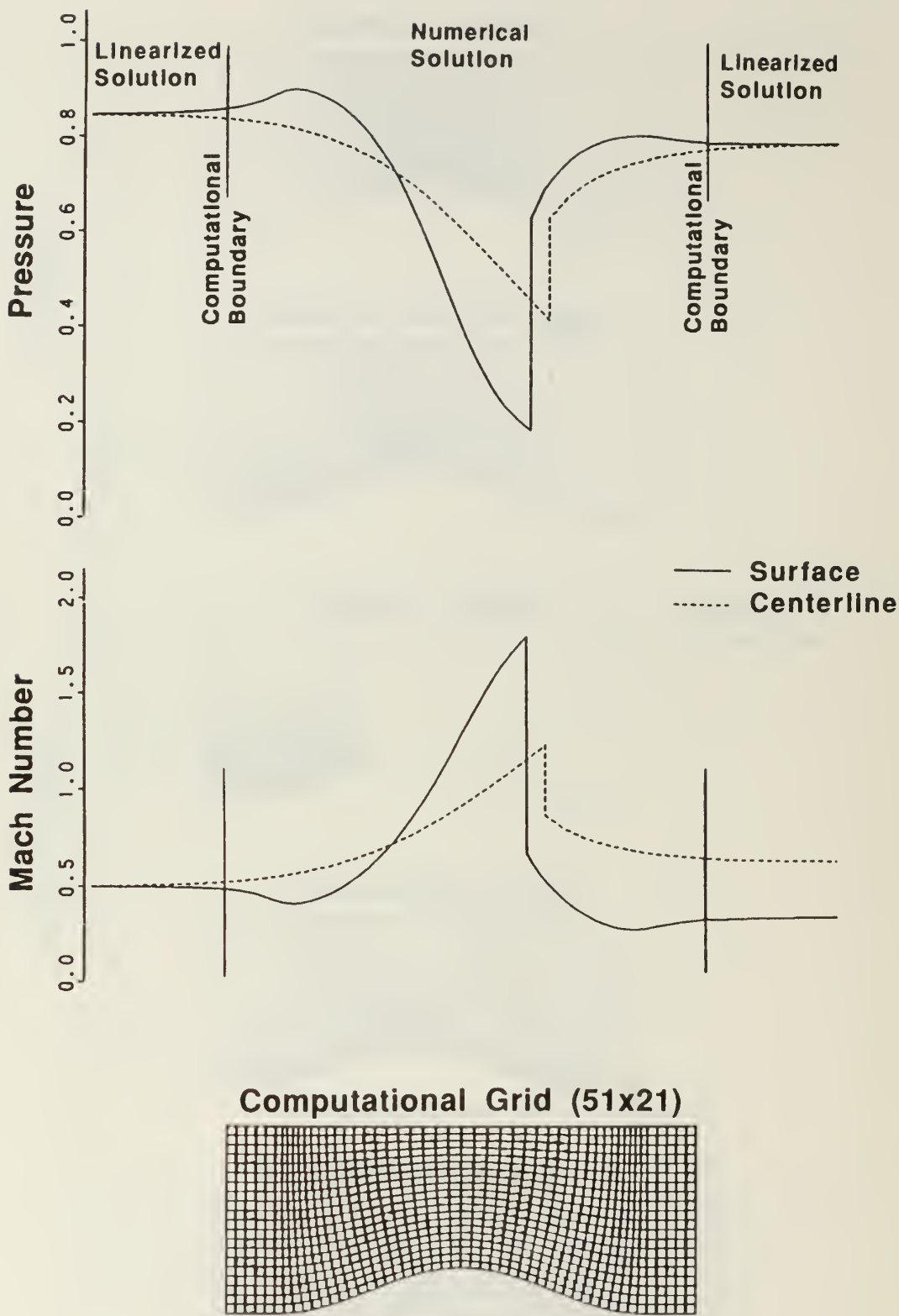
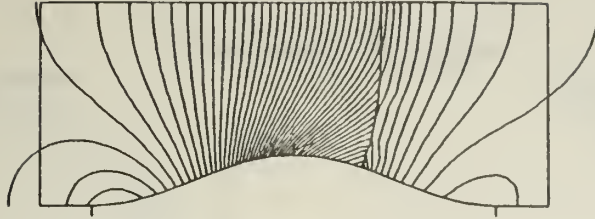
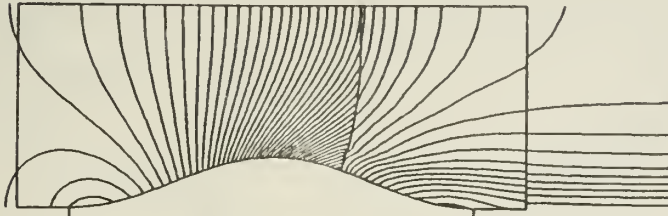


Figure 23. Pressure and Mach Number Distributions
 First-Order Boundary Conditions
 $p_{\infty} = 0.78$

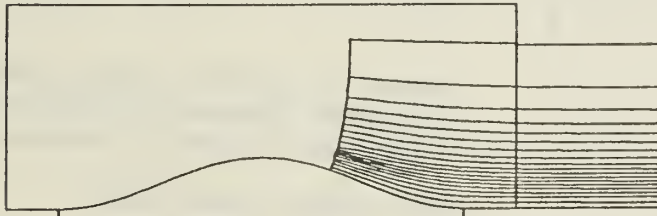
Pressure Contours



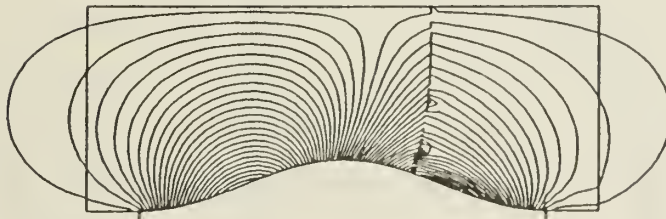
Mach Number Contours



Entropy Contours



Flow Angle Contours



Computational Grid (51x21)

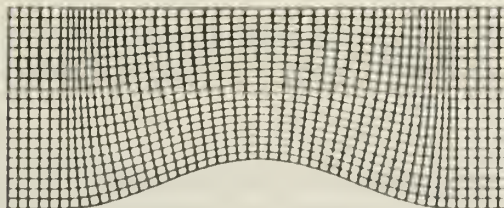
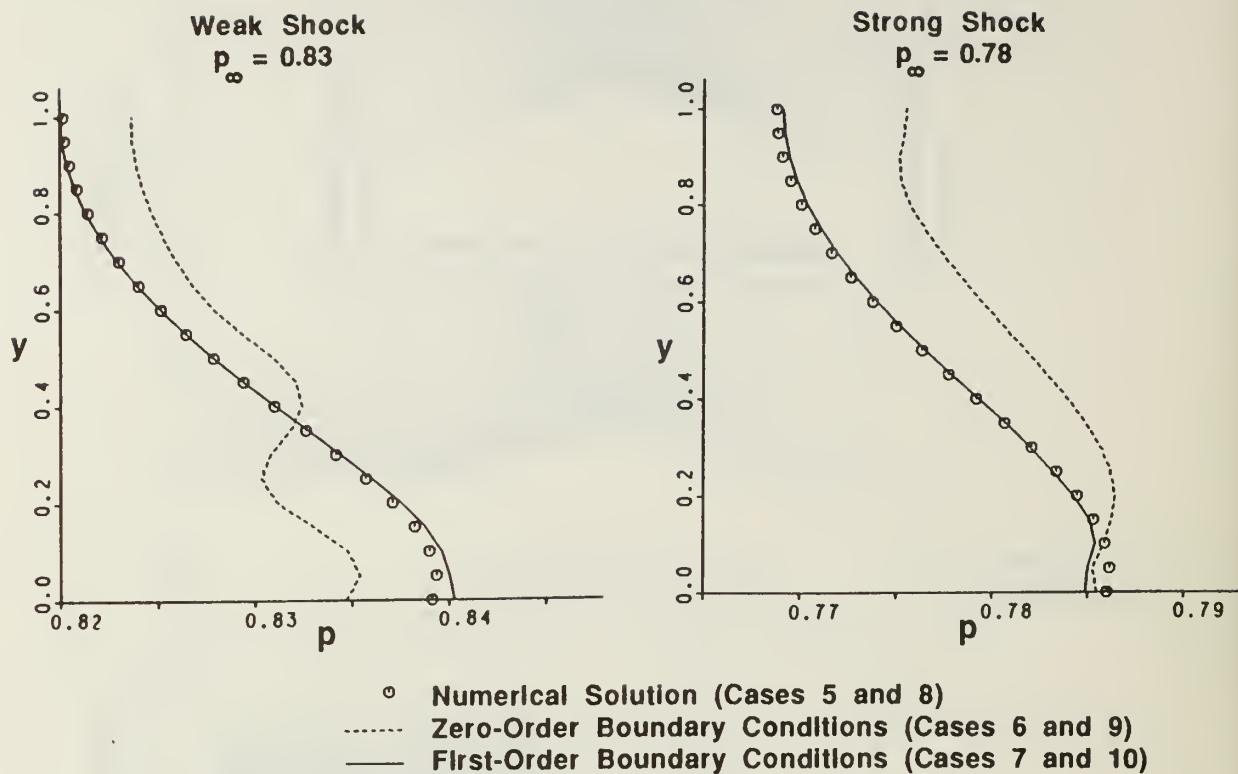


Figure 24. Pressure, Mach Number, Entropy and Flow Angle Contours
First-Order Boundary Conditions
 $p_{\infty} = 0.78$

Pressure Distribution



Flow Angle Distribution

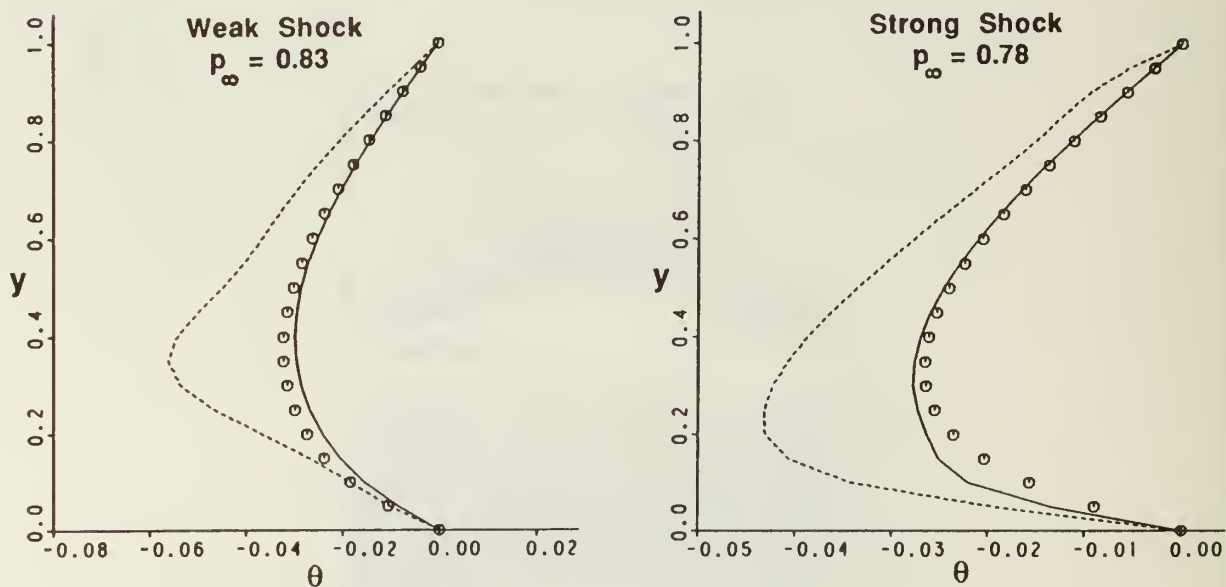


Figure 25. Pressure and Flow Angle Distributions on Downstream Computational Boundary

INITIAL DISTRIBUTION LIST

1. Commander
Naval Air Systems Command
Washington, DC 20361
Attention: Code AIR 931 1
Code AIR 931E 1
Code AIR 530 1
Code AIR 536 1
Code AIR 5004 4
Code AIR 93D 1

2. Office of Naval Research
800 N. Quincy Street
Arlington, VA 22217
Attention: Dr. Jack Hansen 1

3. Commanding Officer
Naval Air Propulsion Center
Trenton, NJ 08628
Attention: G. Mangano, PE-31 1

4. Commanding Officer 1
Naval Air Development Center
Warminster, PA 19112
Attention: AVTD

5. Library 1
Army Aviation Material Laboratories
Department of the Army
Fort Eustis, VA 23604

6. Dr. Arthur J. Wennerstrom 1
AFWAL/POTX
Wright-Patterson AFB
Dayton, OH 45433

7. Air Force Office of Scientific Research 1
AFOSR/NA
Bolling Air Force Base
Washington, DC 20332
Attention: Dr. James Wilson

8. National Aeronautics & Space Administration
Lewis Research Center
21000 Brookpark Road
Cleveland, OH 44135
Attention: Chief, Internal Fluid Mechanics Division 1
Library 1
N. Sanger MS 5-11 1
J. Adamczyk MS 5-11 1
R. Chima MS 5-11 1
P. Sockol MS 5-11 1
J. Sanz MS 5-11 1

- | | | |
|-----|---------------------------------------------------------------------------------------------------------------------------------------------|---|
| 09. | Library
General Electric Company
Aircraft Engine Technology Division
DTO Mail Drop H43
Cincinnati, OH 45215 | 1 |
| 10. | Library
Pratt & Whitney Aircraft Group
Post Office Box 2691
West Palm Beach, FL 33402 | 1 |
| 11. | Library
Pratt-Whitney Aircraft Group
East Hartford, CT 06108 | 1 |
| 12. | Library
Curtis Wright Corporation
Woodridge, NJ 07075 | 1 |
| 13. | Library
AVCO/Lycoming
550 S. Main Street
Stratford, CT 06497 | 1 |
| 14. | Library
Teledyne CAE, Turbine Engines
1330 Laskey Road
Toledo, OH 43612 | 1 |
| 15. | Library
Williams International
P. O. Box 200
Walled Lake, MI 48088 | 1 |
| 16. | Allison Gas Turbine Division
General Motors Corporation
P.O. Box 420
Indianapolis, IN 46206-0420
Attention: Dr. R.A. Delaney | 1 |
| 17. | Library
Garrett Turbine Engine Company
111 S. 34th Street
P. O. Box 5217
Phoenix, AZ 85010 | 1 |
| 18. | Professor J. P. Gostelow
School of Mechanical Engineering
The New South Wales Institute of Technology
New South Wales
AUSTRALIA | 1 |

19. Dr. G. J. Walker 1
 Civil and Mechanical Engineering
 Department
 The University of Tasmania
 Box 252C
 GPO Hobart, Tasmania 7110
 AUSTRALIA
20. Professor F. A. E. Breugelmans 1
 Institut von Karman de la Dynamique
 des Fluides
 72 Chaussee de Waterloo
 1640 Rhode-St. Genese
 BELGIUM
21. Professor Ch. Hirsch 1
 Vrije Universiteit Brussel
 Pleinlaan 2
 1050 Brussels
 BELGIUM
22. National Aeronautics & Space Administration
 AMES Research Center
 Moffett Field, CA 94035
 Attention: Dr. Man M. Rai (RFA:258-D) 1
 Dr. Paul Kutler (RFA:258-D) 1
23. Dr. John Denton 1
 Whittle Laboratory
 Department of Engineering
 Cambridge University
 ENGLAND
24. Library 1
 ONERA
 29, Ave. de la Division Leclerc
 92 Chatillon
 FRANCE
25. Professor D. Adler 1
 Technion Israel Institute of Technology
 Department of Mechanical Engineering
 Haifa 32000
 ISRAEL
26. Dr. P. A. Paranjpe 1
 Head, Propulsion Division
 National Aeronautics Laboratory
 Post Bag 1700
 Bangalore - 17
 INDIA

27. Dr. W. Schlachter 1
Brown, Boveri Company Ltd.
Dept. T-T
P. O. Box CH-5401 Baden
SWITZERLAND
28. Professor Leonhard Fottner 1
Department of Aeronautics and Astronautics
German Armed Forces University
Hochschule des Bundeswehr
Werner Heisenbergweg 39
8014 Neubiberg near Munich
WEST GERMANY
29. Professor Dr. Ing. Heinz E. Gallus 1
Lehrstuhl und Institut fuer Strahlantiebe
und Turbourbeitmashinen
Rhein.-Westf. Techn. Hochschule Aachen
Templergraben 55
5100 Aachen
WEST GERMANY
30. Dr. Ing. Hans-J. Heinemann 1
DFVLR-AVA
Bunsenstrasse 10
3400 Geottingen
WEST GERMANY
31. Dr. H. Weyer 1
DFVLR
Linder Hohe
505 Porz-Wahn
WEST GERMANY
32. United Technologies Research Center
East Hartford, CT 06108
Attention: Dr. R.P. Dring 1
Dr. J. Verdon 1
Dr. R.L. Davis 1
Dr. J.E. Carter 1
33. Director, Gas Turbine Laboratory 1
Aeronautics and Astronautics Department
31-265 Massachusetts Institute of Technology
Cambridge, Massachusetts 02139
34. Dr. B. Lakshminarayana 1
Professor of Aerospace Engineering
The Pennsylvania State University
233 Hammond Building
University Park, Pennsylvania 16802

35. Mr. R. A. Langworthy 1
Army Aviation Material Laboratories
Department of the Army
Fort Eustis, VA 23604
36. Mechanical Engineering Department
Virginia Polytechnic Institute and
State University
Blacksburg, VA 24061
Attention: Professor W. O'Brian 1
Professor H. Moses 1
Professor J. Moore 1
37. Professor T. H. Okiishi 1
Professor of Mechanical Engineering
208 Mechanical Engineering Building
Iowa State University
Ames, Iowa 50011
38. Dr. Fernando Sisto 1
Professor and Head of Mechanical
Engineering Department
Stevens Institute of Technology
Castle Point
Hoboken, NJ 07030
39. Dr. Leroy H. Smith, Jr. 1
Manager, Compressor and Fan
Technology Operation
General Electric Company
Aircraft Engine Technology Division
DTO Mail Drop H43
Cincinnati, OH 45215
40. Dr. W. Tabakoff 1
Professor, Department of Aerospace
Engineering
University of Cincinnati
Cincinnati, OH 45221
41. Mr. P. Tramm 1
Manager, Research Labs
Detroit Diesel Allison Division
General Motors
P. O. Box 894
Indianapolis, IN 46206
42. Mr. P. F. Yaggy 1
Director
U. S. Army Aeronautical Research Laboratory
AMES Research Center
Moffett Field, CA 94035

43.	Defense Technical Information Center Cameron Station Alexandria, VA 22314	2
44.	Naval Postgraduate School Monterey, CA 93943-5100 Attention: Professor M. F. Platzer (67P1) Turbopropulsion Laboratory (67Sf) Library (1424) Research administration (012)	1 15 2 1
45.	Dr. August Verhoff McDonnell Aircraft Company Mail Code: 341/32/2/MS122 P.O. Box 516 St. Louis, MO 63166	30
46.	Dr. Steven Shamroth Scientific Research Associates P.O. Box 498 Glastonbury, CT 06033	1
47.	Dr. Chunill Hah General Electric Company CR & D K-1 Schenectady, NY 12345	1

DUDLEY KNOX LIBRARY



3 2768 00336443 1